MICROCOPY RESOLUTION TEST CHART

NATIONAL BUREAU OF STANDARDS-1963

AD-A179 231

EVALUATION OF TERSOFF'S REVISED SILICON
POTENTIAL IN A MOLECULAR DYNAMIC
SIMULATION OF SOLID SILICON

THESIS

William D. Metzler
Captain, USAF

AFIT/GNE/ENP/87M-5

DEPARTMENT OF THE AIR FORCE

AIR UNIVERSITY

AIR FORCE INSTITUTE OF TECHNOLOGY

Wright-Patterson Air Force Base, Ohio

87 4 13 0

EVALUATION OF TERSOFF'S REVISED SILICON
POTENTIAL IN A MOLECULAR DYNAMIC
SIMULATION OF SOLID SILICON

THESIS

William D. Metzler
Captain, USAF

AFIT/GNE/ENP/87M-5

DTIC
SELECTED
APR 1 7 1987
E

Approved for public release;   distribution unlimited

EVALUATION OF TERSOFF'S REVISED SILICON POTENTIAL

IN A

MOLECULAR DYNAMIC SIMULATION OF SOLID SILICON

THESIS

Presented to the Faculty of the School of Engineering

of the Air Force Institute of Technology

Air University

In Partial Fulfillment of the

Requirements for the Degree of

Master of Science in Nuclear Science

William D. Metzler, B.S.

Captain, USAF

March 1987

Approved for public release; distribution unlimited

Preface

The purpose of this study was to evaluate the Tersoff silicon potential for use in Molecular Dynamic simulations. There has been a great deal of interest in silicon modeling in recent years, but a successful, general purpose temperature independent silicon potential has so far eluded researchers. Although the focus of this work was looking toward melting/annealing studies to model the reversible crystal/amorphous transition, a general purpose silicon potential would be useful in modeling the thin-layer plating of silicon (for electrical component design) and a host of other interesting characteristics.

While the results of this particular study were not favorable, the general feeling among many researchers is that the Tersoff style of potential holds a great deal of promise. Since a molecular dynamic/static computer code already exists, I hope this study is continued by following students. The two appendices included at the end of this report should help following students to understand the specifics of the code begun by Paul Thee in his thesis.

Three people have provided invaluable aid in the completion of this research. The first is Capt. Michael Sabochick, who was always willing to set aside other equally important projects to explain, discuss, or brain-storm various aspects of this project. A second indespensable

Table of Contents

List of Figures

List of Figures

List of Tables

Abstract

The goal of this research was to provide an initial
testing of a new silicon potential proposed by Tersoff.
Molecular Dynamic (MD) simulations were performed at four
temperatures below the melting point of silicon to evaluate
the new potential's ability to reproduce the characteristics
of diamond-Si. A constant enthalpy ensemble composed of 64
atoms was used for the evaluation.

Although the Tersoff potential does identify the diamond
structure as the lowest energy crystal at absolute zero,
problems were noted at higher temperatures. At all
temperatures above zero, the calculational cell showed a
marked decrease in volume. The amount of system shrinkage
increased with increasing simulation temperature. Because
of this shrinkage, the Tersoff potential is unusable in MD
simulations.

Several attempts were made to isolate and identify the
cause of the shrinkage, but were unsuccessful. It was noted
that as the bonding environment became more favorable
(stronger bonding), the bonding radius of minimum energy
decreased. Since the potential relies primarily on
coordination number to stabilize the diamond structure,
it is postulated that there exists an as-yet unidentified
four-bond configuration that provides a lower energy and as
a result has a shorter rest bond length than the tetrahedral
diamond structure.

ix

EVALUATION OF TERSOFF'S REVISED SILICON POTENTIAL

IN A MOLECULAR DYNAMIC SIMULATION OF SOLID SILICON

I. Introduction

Background

Since its inception in 1959 (1), molecular dynamics
(MD) has become a very popular research tool for the study
of material properties (3 - 5, 7, 11, 14). Unlike Brownian
dynamics or Monte-Carlo techniques, MD solves Newton's
equation of motion to produce a strictly deterministic
simulation of the trajectories of the individual atoms in
the model volume. Monitoring the movement of each atom as
it interacts with neighboring atoms through a pre-
established interatomic potential permits researchers to
study the mechanics of effects observed in the laboratory,
and provides information unavailable from traditional
measurement methods (11:799). Additionally, MD offers
complete control of the environment, allowing the user to
observe material behavior under conditions that would be
difficult or impossible to create in a laboratory (8:1).

Before this powerful tool can be used to simulate a
actual system, however, an accurate interatomic potential
function for the material must be determined. Past studies
have relied heavily on pair potentials (6, 7, 9, 11). The

1
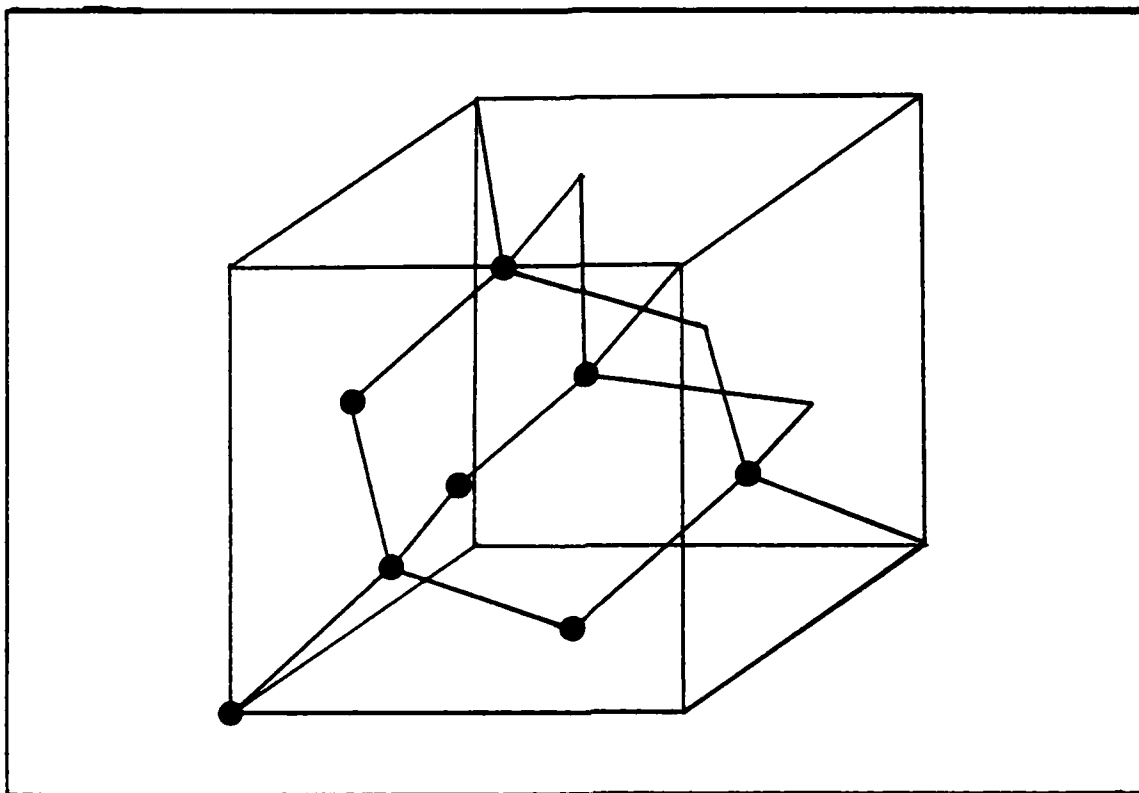
Figure 1: Diamond Structure for Silicon

advantage of pair potentials is that they are relatively
simple and computationally less demanding than more general
potential functions, but still allow accurate modeling of
noble materials. However, one common feature of all pair
potentials is spherical symmetry. This makes them
unsuitable for modeling materials that display directional
covalent bonding, such as silicon. Pair potentials fail to
stabilize the diamond crystalline structure observed in
natural silicon (Figure 1), and degeneration to a hexagonal
close pack (HCP) structure is observed (3:2001).

A significant amount of research effort has been
expended in the development of an accurate interatomic
potential function for silicon. Several new potentials have

been devised, with most being three-body potentials (3, 13, 15). These three-body potentials provide stability to the diamond crystal structure, but required calculations for most three-body interactions scale as N^3, where N is the number of particles. The resulting computational demand limits the practical size of systems that can be studied. The Biswas and Hamann potential is an exception, because the separable form of their function allows N^2 scaling (3:2001).

The Tersoff silicon potential offers a notably different approach to the problem of silicon modeling. Tersoff has avoided explicit three-body terms in the potential, resulting in a hybrid two-body potential in which the attractive term is modified by the bonding environment. Because the Tersoff potential is basically a two-body potential, the bond calculations scale as N^2 rather than N^3. Since processor time is a major limitation in MD studies, this is a very attractive feature. In addition, this potential includes structural information that may allow its use in studies where silicon structures other than diamond are to be examined. The specifics of the Tersoff potential are discussed in Chapter II.

To date, Tersoff has proposed two different silicon potentials, the second representing a modification of the original. Tersoff's initial silicon potential (16) was evaluated in a molecular dynamic simulation by Thee (18). One major problem with the original potential identified in Thee's work was that the atom density increased with

increasing temperature up to 1000° K, contrary to known
behavior of silicon (19). As a result, the original
potential was deemed unusable in MD simulations. Tersoff's
modified potential function (17) was investigated in this
work.

Problem Statement

The purpose of this research was to determine the
usefulness of the new Tersoff potential for MD simulations.
This represents an initial step toward the ultimate goal of
simulating the melting and annealing behavior of silicon
undergoing pulsed laser heating. The melting/annealing of
silicon is of particular interest to the military as a
survivable means of mass information storage. Because of
its annealing characteristics, silicon has been widely used
as an optical storage medium. Advantages of optical storage
include very high data density (> 10^{8} bits/cm^{2}), faster
access time, and resistance to EMP (electromagnetic pulse -
a nuclear blast effect), unlike the magnetic storage media
now in wide useage. By studying the mechanics of silicon
annealing, better optical storage designs may be possible.

Scope

This work was limited to an initial examination of the
new Tersoff silicon potential. Other current potentials
were not evaluated, and no melting/annealing behavior was
tested. Because this represented only a "proving" of the

4

potential, the simulation was limited to 64 atoms to expedite the results, and periodic boundary conditions were used to arrive at bulk properties. Therefore edge effects and boundary phenomenon were not examined.

Assumptions

As with any simulation, numerous assumptions and approximations were required to make this problem manageable. Rather than being identified in this section, required simplifications are discussed in the relevant portions of the following chapters, where the accompanying discussion should provide the reader with a better understanding of their effects.

Round-off errors are the single exception. The majority of experimental runs completed in this research effort were performed on a Cray X/MP computer. This machine uses 14 significant digits in single precision, more than sufficient to keep round-off errors negligible, even over thousands of time-steps. The remaining runs were completed on a VAX 11/780 in double-precision mode. This provided 16 significant digits in the numerical calculation, but the increased processing time made it impractical to use the VAX computer for the majority of the tests run.

General Approach

This research effort was completed in four stages. The first stage, consisting primarily of computer coding, involved modification of Thee's existing molecular dynamics

code (14) to include the new Tersoff potential and appropriate derivatives. Once coding was completed, several test runs were performed to insure the potential and positional derivatives (forces) were correct. This validation of the code comprised stage two of the research. Stage three included the full-scale tests of the silicon model at temperatures below melting to evaluate the ability of the simulation to reproduce the physical behavior of solid silicon in a diamond configuration. Study and analysis of the changes in lattice structure as a result of heating concluded the research.

Sequence of Presentation

The final report on this research effort is divided into six chapters. Chapter I is the introduction, which presents a brief history of the development of the silicon potential and outlines the research procedure. Chapter II describes in detail Tersoff's new potential. Computational techniques used to perform the simulation and procedures used to calculate the material properties are described in Chapter III. Chapter IV contains the results of both the test runs used to validate the code and the evaluation runs, which were completed at four selected temperatures well below the melting point for silicon. Behavioral analysis of the potential is undertaken in Chapter V. The conclusions resulting from this work and recommendations for future efforts are the subject of Chapter VI.

II. Tersoff's Modified Silicon Potential

Interatomic Potentials (General)

In developing an interatomic potential, it is generally assumed that the potential energy at any point in space can be expressed as a sum of contributions from individual x-body interactions. For a system containing N identical atoms, the total potential energy U for the system could be written (15:5262)

$$U(1,\ldots,N) = \sum_i u_1(r_1) + \sum_{\substack{i,j \\ i<j}} u_2(r_1,r_j)$$

$$+ \sum_{\substack{i,j,k \\ i<j<k}} u_3(r_1,r_j,r_k) +\ldots+ u_N(r_1,r_2,\ldots,r_N) \quad (1)$$

where r_1 is the position vector for atom i, and u_x is the potential energy due to x-body interactions, which is a function of the position of the x atoms. The first term on the right hand side of (1) describes the potential due to the external environment, and is of no concern in this work. Therefore the first applicable term in equation (1) is the pair potential u_2, which is summed over all atom pairs. The u_3 term describes the potential energy due to all possible three body interactions, and additional terms are necessary for the higher order interactions. The final term u_N describes the energy due to the single arrangement involving all N atoms of the system.

7

incorporating both the two- and three-body terms of equation
(1). The basic weakness in these potentials is that they
are generally fit specifically to the diamond structure of
silicon, and have very limited application in simulating
other silicon structures (5:7363).

The Tersoff potential, on the other hand, explicitly
accounts for the bonding environment, relying on control of
the coordination number as described below to stabilize the
diamond structure. This approach offers the possibility of
a much more widely applicable silicon potential.

Tersoff's New Silicon Potential

The form of the Tersoff potential was motivated "by
intuitive ideas about the dependence of bond order upon the
local environment" (16). The general form of the potential,
as previously mentioned, is a modified pair potential very
similar to the Morse potential (16). Tersoff's proposed
two-body potential is

$$U = \sum_{\substack{i,j \\ i<j}} u_2(r_{ij}) = 1/2 \sum_{\substack{i,j \\ j \neq i}} u_2(r_{ij}) \qquad (2)$$

where the pair potential u_2 is a function of the separation
distance r_{ij} between atoms i and j such that

$$u_2(r_{ij}) = f_c(r_{ij})[A \exp(-\lambda_1 r_{ij}) - B_{ij}\exp(-\lambda_2 r_{ij})] \qquad (3)$$

The $f_c(r_{ij})$ term is the cut-off function used to limit the
range of the potential, and B_{ij} contains the bonding

Table I: Parameter Values for Tersoff's Silicon Potential

Variable	Value	Variable	Value
A	3264.65 (eV)	n	22.9559
B_0	95.3727 (eV)	R	3.0 (A)
b	1.40949E-11	D	0.2 (A)
c	4.83810	λ_1	3.23940 (/A)
d	2.04167	λ_2	1.32583 (/A)
h	8.80498E-6	λ_3	3.23940 (/A)

----

environment information as defined below. The variables A,
λ_1, and λ_2 were chosen to provide correct bond energy and
bond length for silicon diamond, FCC, and simple cubic
structures, as well as other static properties not
specifically identified by Tersoff in his communiqué. The
values reported by Tersoff for these variables (and others
to be introduced later) are recorded in Table I.

   Cut-off Function f_c. The cut-off function provides a
dual service. It limits the range of the interaction to a
reasonable distance and simultaneously provides for
continuous spatial derivatives so that forces can be
calculated (see Figure 2). The particular form of the
cut-off function used by Tersoff is

$$f_c(r) = \begin{cases} 1, & r < R - D \\ .5 - .5\sin[\dfrac{\pi(r - R)}{2D}], & R - D < r < R + D \quad (4) \\ 0, & r > R + D \end{cases}$$
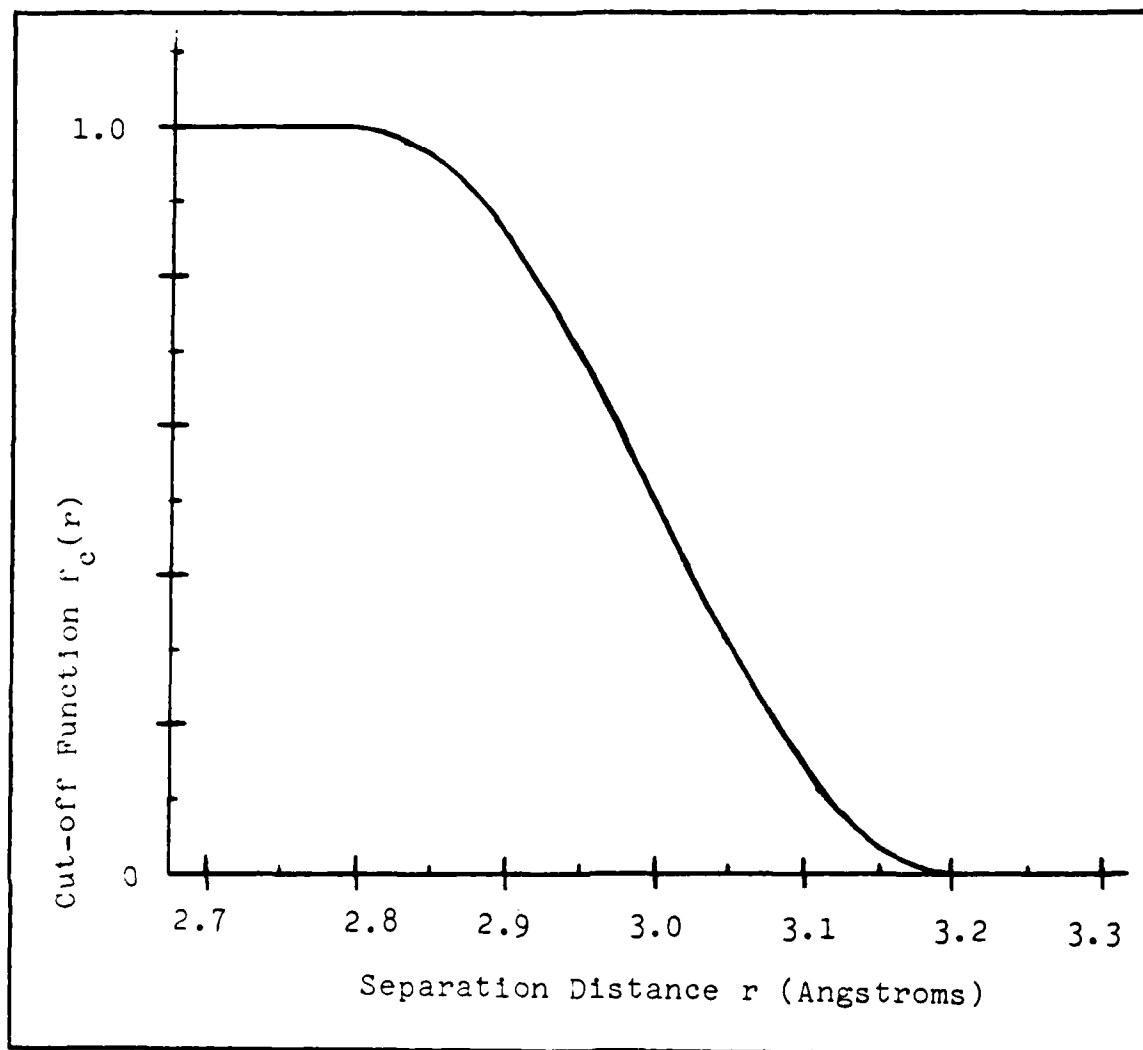
Figure 2: Cut-off Function vs. Separation Distance

where r is the distance in angstroms separating the atoms of
interest. The selected values for R and D are included in
Table I. For a lattice constant of 5.4312 angstroms (solid
silicon at 300 degrees K), the 3.2 angstrom cut-off radius
falls between the nearest neighbor distance (2.35 angstroms)
and the next-nearest neighbor distance (3.84 angstroms).

Environmental Factor B_{ij}. The environmental effect on
bond strength is reflected in the B_{ij} term. This term was
the focus of Tersoff's modification of his original silicon

11

potential (16). Only the modified potential which was the basis of this study will be discussed here. Interested readers are referred to the original article to compare the two potentials.

The value of B_{ij} for any bonded i-j pair is found by

$$B_{ij} = B_0(1 + bz_{ij}^n)^{-1/(2n)} \tag{5}$$

Values for B_0, b, and n can be found in Table I. The z_{ij} term contains the bonding environment information, and is defined by

$$z_{ij} = \sum_{k \neq i,j} f_c(r_{ik})g(\Theta)\exp\{-[\lambda_3(r_{ik} - r_{ij})]^3\} \tag{6}$$

where the summation is over all k atoms for the given i-j pair. The cut-off function f_c is as previously defined and the $g(\Theta)$ function contains the angular dependence in the potential.

$$g(\Theta) = 1 + \left(\frac{c^2}{d^2}\right) - \frac{c^2}{d^2 + [\cos(\Theta) + h]^2} \tag{7}$$

Theta is the angle between the i-k and i-j bonds, and the values of the empirical parameters λ_3, c, d, and h are contained in Table I.

The calculation of B_{ij} presents a possible problem in computer simulations. For configurations where $r_{ik} \gg r_{ij}$, the value of z_{ij} can become quite large (on the order of 10^8). When this is then raised to the n-th power (n $\approx$ 23)

12

for the computation of B_{ij}, the capabilities of the computer

may be exceeded. This can be avoided by noting that when

z_{ij} becomes large, equation (5) can be simplified to

$$B_{ij} = B_0\ b^{-1/(2n)}\ z_{ij}^{-1/2} \qquad\qquad (5a)$$

with negligible loss of accuracy. This approximation was

used to evaluate B_{ij} for large values (> 5) of z_{ij}.

Figure 3 gives a visual representation of the effect of

changing environment on bond strength. Two trends should

be noted in Figure 3. First, the larger the B_{ij} term is,

the lower the bond energy (stonger bonding) for any

separation distance. Second, as B_{ij} decreases, the most

favored (lowest energy) bond length increases. Therefore

both bond energy and preferred bond length are functions of

the bonding environment.

Coordination Number vs. Bond Strength. The competition

between coordination number and bond strength is of primary

importance in determining the bond environment as

represented by the B_{ij} term. Increasing coordination

requires more i-j bonds, each of which contributes to the

overall system energy. Since bond energies are negative,

a greater number of bonds equates to a lower (greater

negative) energy and therefore a more stable configuration.

This is the case with ordinary pair potentials. In

Tersoff's potential, however, increasing coordination number

also increases the number of terms in the summation of z_{ij},

13
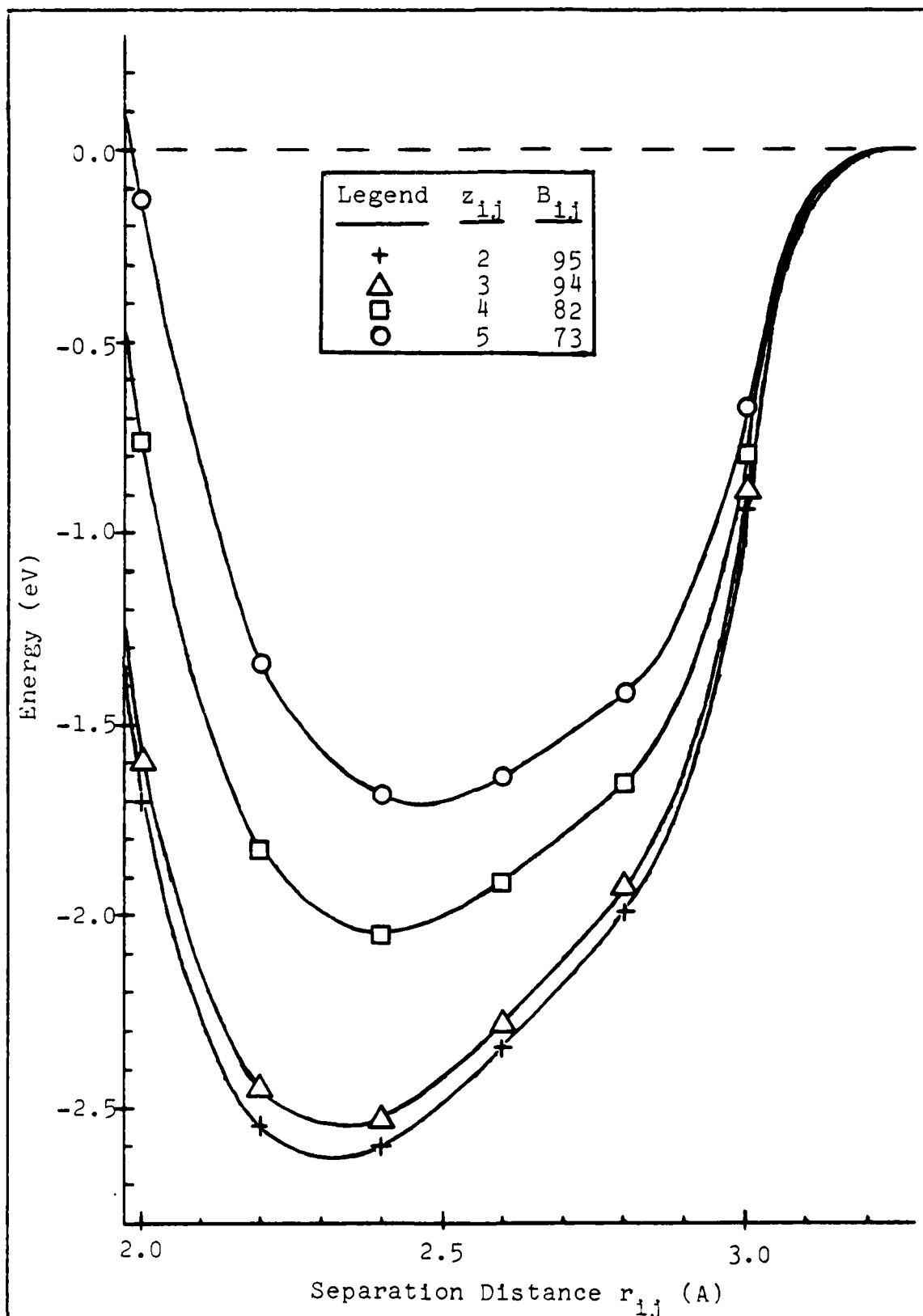
Figure 3: Potential Energy of a Single Bond vs. Separation Distance r_{ij} for Small Values of z_{ij}
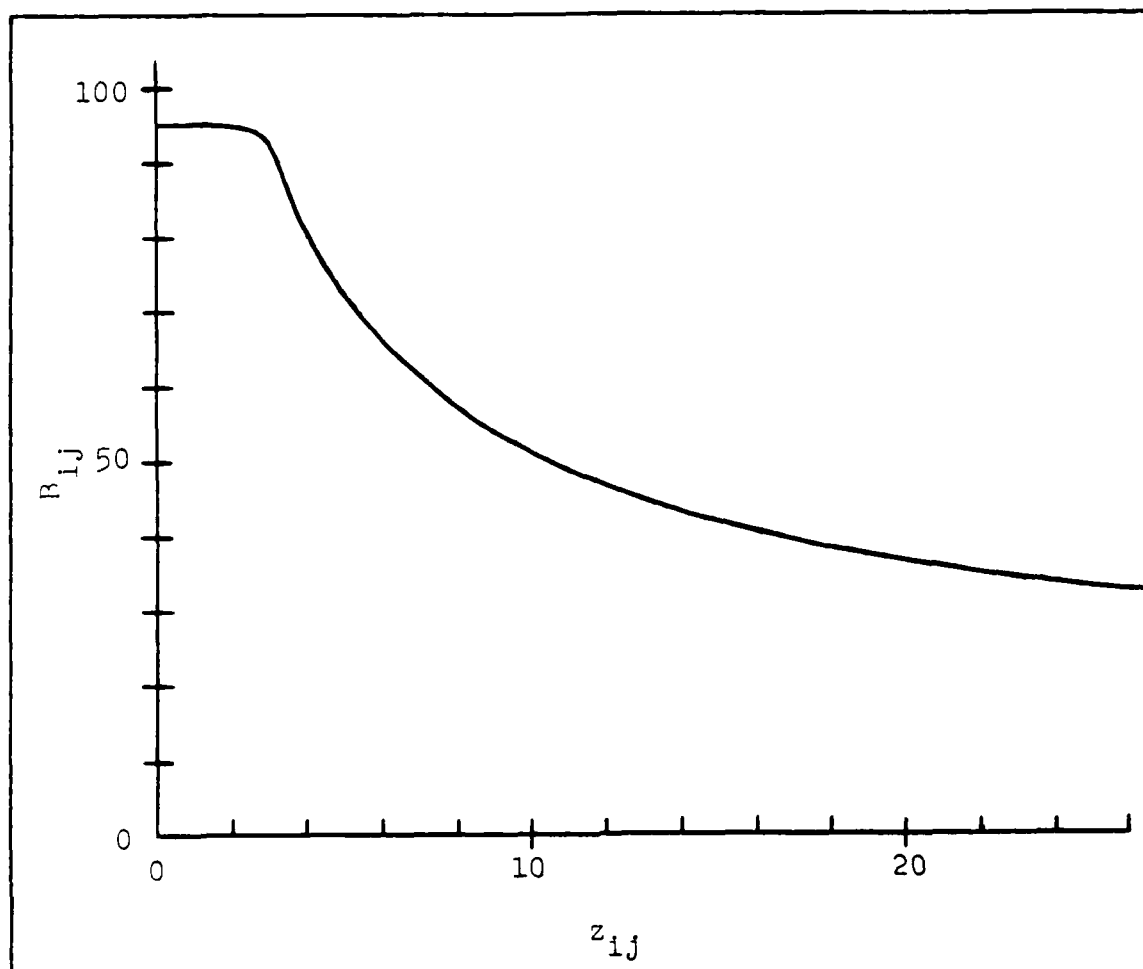
Figure 4: B_{ij} vs. z_{ij}

which increases z_{ij} and decreases B_{ij} (see Figure 4). The decrease in B_{ij} results in a weaker (less negative) bond energy for each individual i-j bond, therby countering the effect previously discussed. This attempt to model the response of silicon-silicon bonding to changes in the environment provides the major differentiation between the Tersoff potential and other potentials.

Angular Dependence. The angular dependence seems to have only a marginal effect on the bond strength. The rapid increase in z_{ij} with increasing coordination number is the
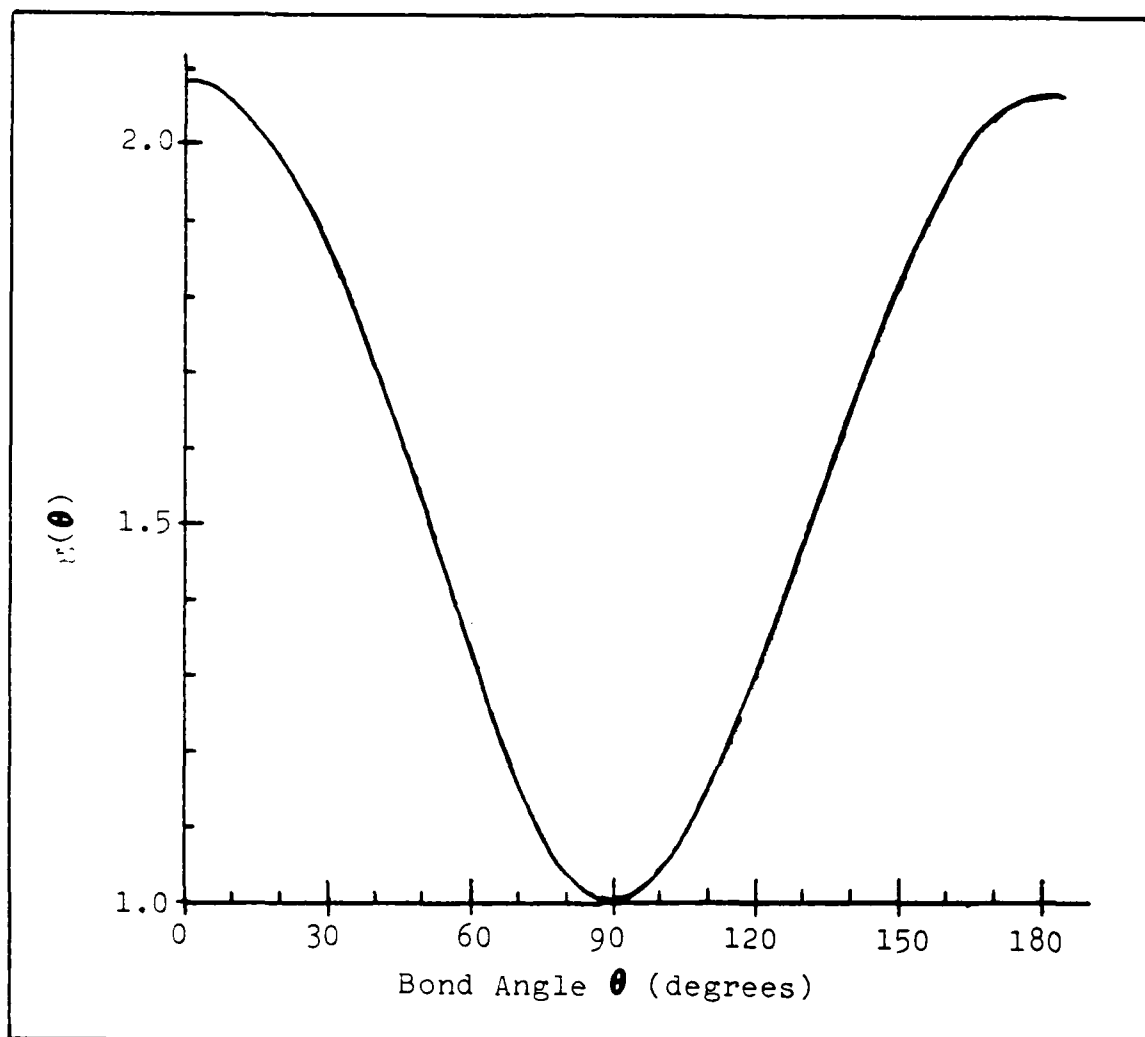
Figure 5: Angular Dependence of g(Θ) Function

primary tool used to stabilize the diamond structure within Tersoff's potential. The weak dependence of g(Θ) on the bonding angle Θ (see Figure 5) is a result of Tersoff's empirical fitting of the potential to several static crystal structures, and offers the possibility of a potential applicable to many different silicon structures.

III. Molecular Dynamic Model

The purpose of this chapter is twofold: 1) to provide
the reader with a brief overview of the process of molecular
dynamic simulation to allow better understanding of the
results reported; and 2) to explain briefly the calculations
required to convert the results of a MD simulation into the
material properties reported in the following chapters.
If a further explanation of MD or statistical mechanics is
desired, the reader is referred to texts 8 and 10 listed in
the Bibliography.

Overview of Molecular Dynamics (MD)

The purpose of the molecular dynamic simulation is to
solve Newton's equation of motion for each particle in the
simulation volume, providing a time-history of each
particle's position and velocity over the period of the
simulation. For a system of N identical atoms, this
requires the solution for each time step of a set of N
differential equations of the form

$$m_i \frac{d}{dt}(\bar{v}_i) = \bar{F}_i = - \frac{d}{d\bar{r}_i}[U(\bar{r}_N)] \tag{8}$$

where m_i, $\bar{v}_i$, and $\bar{r}_i$ are the mass, velocity, and position
of atom i, respectively, $U(\bar{r}_N)$ is the total potential energy
of the system as a function of the N atomic positions, and
$\bar{F}_i$ is the total force on atom i.

17

Analytical solution of the set of differential equations described by (8) above would be impossible in a practical sense. Instead, the Gear Predictor-Corrector Algorithm as described by Haile (8:17) was used to provide a numerical solution. Because this calculation is the heart of the MD simulation, a brief explanation of the procedure will be presented here.

Gear Predictor-Corrector Algorithm (GPCA). Given the positions $\bar{r}_i$ and first five time derivatives $\bar{r}_i^{(1)}$, $\bar{r}_i^{(2)}$, $\bar{r}_i^{(3)}$, $\bar{r}_i^{(4)}$, and $\bar{r}_i^{(5)}$ for each of the N atoms at a given time t_0, the GPCA determined the atom positions at the next incremental time $t' = t_0 + dt$ through a three step process of prediction, evaluation, and correction.

Prediction. A fifth order Taylor expansion was used to predict the position and first five time derivatives for each atom at time t' based on the values at t_0. The predicted value of the n-th time derivative of the position vector for atom i at t' was calculated by

$$p\bar{r}_i^{(n)}(t') = \sum_{k=0}^{5-n} \bar{r}_i^{(n+k)}(t_0) \frac{dt^k}{k!} \qquad (9)$$

where $p\bar{r}^{(n)}(t')$ was the predicted derivative value, dt was the time step size, and $\bar{r}_i^{(n)}(t_0)$ was the n-th time derivative of the position vector for atom i at t_0.

Evaluation. Once the position of each atom was predicted for t', the resultant potential energy and the

18

force on each atom was calculated using Tersoff's potential
function (see Appendix A for derivation of forces). The
calculated atomic forces were divided by the atomic mass to
determine the actual acceleration $\bar{r}_i^{(2)}(t')$ of each atom.
The evaluation of forces was the most computationally
demanding section of the MD simulation, and several time-
saving techniques were included in the model to minimize the
number of required calculations. The computer code used in
this work was a modification of the code used by Thee, whose
thesis provides a detailed explanation of these techniques
(18). The explanation will not be repeated in this work.

Correction. As a result of the evaluation step,
the actual acceleration of each atom at t' was known. The
difference between the predicted and actual accelerations
for each atom defined N error terms $dr_i^{(2)}(t')$ by

$$dr_i^{-(2)}(t') = \bar{r}_i^{(2)}(t') - p\bar{r}_i^{(2)}(t') \qquad (10)$$

These error terms were then utilized to correct the
predicted positions and remaining four time derivatives of
each atom according to the relationship

$$\bar{r}_i^{(n)}(t') = p\bar{r}_i^{(n)}(t') + a_n d\bar{r}_i^{(n)}(t') \qquad (11)$$

The a_n coefficients in equation (11) provide numerical
stability to the solutions of the differential equations and
vary with the order of the predictor. Coefficients for the
fifth order Taylor expansion used in this study are listed

19

Table II: Values of Coefficients for 5th Order GPCA

Coefficient	Value	Coefficient	Value
a_0	3/16	a_1	251/360
a_2	1	a_3	11/18
a_4	1/6	a_5	1/60

in Table II. The corrected atomic positions and derivatives
as calculated from equation (11) then became the initial
values for the next time increment, and were stored to
provide the time-history needed for property calculations.

   Boundary Conditions and Selection of N. The selection
of the size of the calculational cell (number of atoms N)
used in the MD simulation represented a compromise between
the greater realism of a system containing a large number of
atoms and the lighter computational requirements (faster run
times) of a smaller system. With small systems, however,
only a fraction of the atoms experience the normal 4-atom
coordination. As a result, edge effects would have
overwhelmed the bulk properties of interest without
compensation for the under-coordinated atoms.

   Periodic boundary conditions were used to eliminate
these edge effects, as is common in MD simulations of this
type. By surrounding the calculational cell with exact
images of itself, the proper coordination was provided
for each atom in the cell. Figure 6 shows a two-dimensional
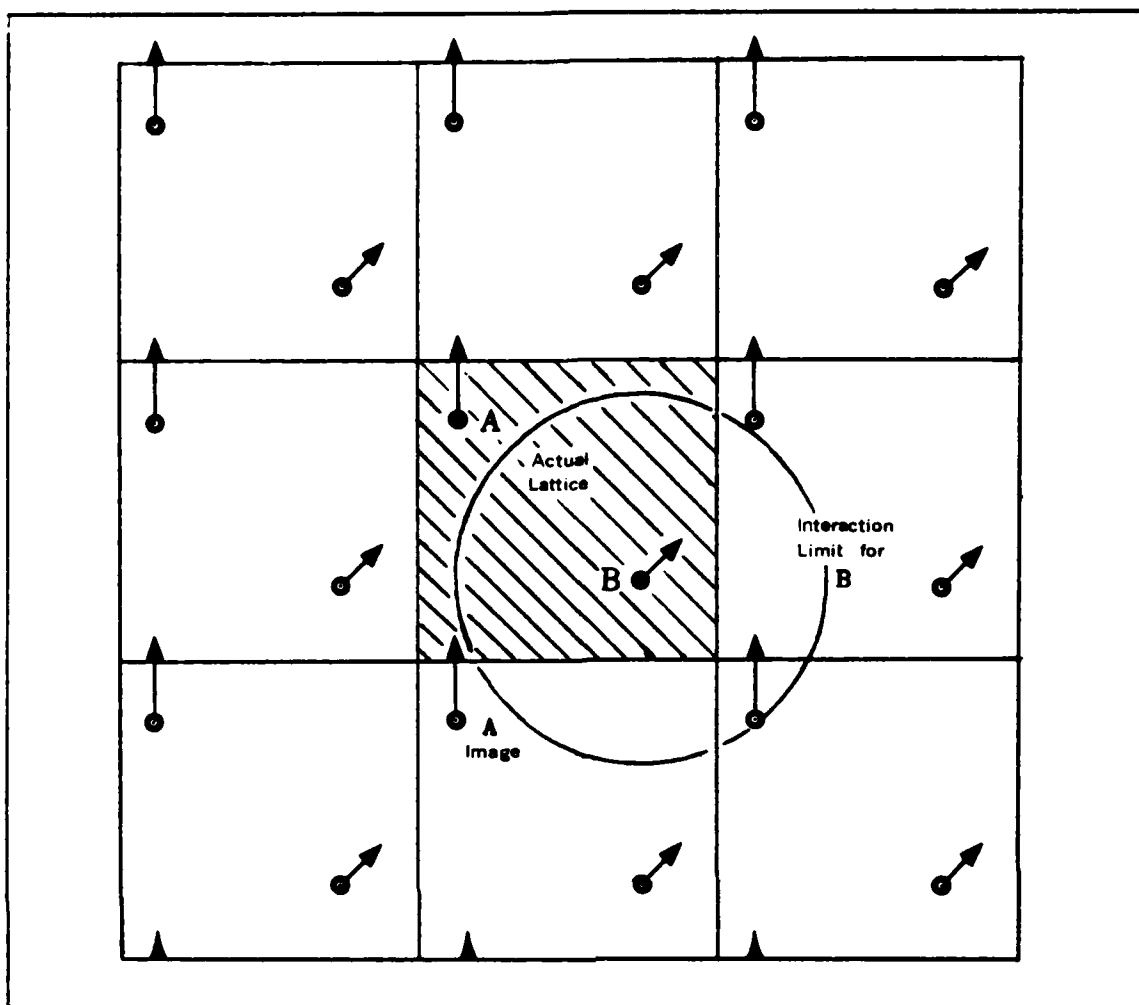
Figure 6: Two Dimensional Periodic Boundaries and Image
Interaction (arrows indicate velocities) (18)

example of periodic boundaries, indicating the interaction

of an atom in the calculational cell with one image of

another atom. The presence of these "images" set a lower

limit on the size of the calculational cell. To provide

stability, the calculational cell had to be large enough to

prevent any atom from simultaneously interacting with more

than one "image" of any neighboring atom. A more complete

explanation of the implementation of periodic boundary

conditions is available in Thee's previous work (18), and

interested readers are directed there for more detail. For
the purpose of this research, 64 atoms in a 2x2x2 array of
diamond lattices was selected as an optimum size for the
calculational cell. This kept run times acceptable, yet was
large enough to remain stable.

Running the Simulation. The actual operation of the MD
simulation was divided into four time phases.

     1.   Initialization

     2.   Scaling Steps

     3.   Resting Steps

     4.   Property Calculation Steps

Each time phase will be discussed separately.

Initialization. To begin a run, the 64 atoms
comprising the computational cell were assigned positions
corresponding to the lattice sites in a diamond crystal,
and three random velocities (one for each directional
component) were generated for each particle. The random
velocities were scaled so that the linear momentum of the
system was zero to prevent net translational motion from
causing erroneous temperature calculations. The computer
code used in this work also allowed the user to save the
positions and velocities from one run and use them as the
initial conditions for a following run, minimizing the
initial shock to the system when runs at high energy
(temperature) are performed. This option was seldom used,
and the results from runs begun in this manner will be so
annotated. After assigning random velocities, the remaining

time derivatives were initially set to zero. This caused

errors in the initial steps of the GPCA, but the derivatives

qu..kly corrected themselves as the simulation progressed.

Scaling Steps. The purpose of the scaling steps

was to establish the desired energy level in the system.

Since temperature is related to the kinetic energy of the

constituent atoms, the simplest method of controlling the

energy was to scale the velocities of the individual atoms

so that the desired temperature was achieved. The

progression of the simulation then partitioned the resulting

total energy between potential and kinetic components. The

number of scaling steps required to stabilize the system

depended on both the amplitude and the level of accuracy

desired in the final temperature, but normally a few tens to

a few hundred steps were sufficient.

Resting Steps. Abrupt termination of scaling

subjects the system to a mild shock (8:28). The purpose of

the resting steps (generally a few tens to a few hundred)

was to allow this shock to dissipate before property

calculations were begun.

Property Calculation Steps. The property

calculation steps generated the actual data from the MD

simulation. The instantaneous property values over several

thousand time steps provided the data base necessary to

calculate the bulk properties of the silicon model. The

actual calculations required to transform the instantaneous

values into bulk properties will be presented later.

Ensembles Used and Time Step Size dt. In describing a system of atoms, the six state variables of density, pressure, volume, temperature, enthalpy, and internal energy can all be calculated if any three are known. MD simulations are generally identified by the three fixed state variables. In this study, two types of ensembles were used, and each will be described separately. The choice of ensembles was found to effect the size of time step that could be used in a simulation. Ideally, one would like to use as large a time step as possible to simulate the longest period of real time in the shortest number of time steps. However, at some maximum allowable time step size, the numerical solution to the differential equations become unstable and the model fails. Time step size and acceptance criterion for each ensemble is discussed below.

(N,V,E) Ensemble. The traditional use of MD was limited to a "micro-canonical" ensemble where atom number, volume, and total energy were held constant. During the course of the simulation, kinetic energy (or instantaneous temperature) and potential energy should both fluctuate around average values out of phase with one another, so that the total energy remains constant. The acceptable amount of variation in the total energy was selected to be 1 part in 10^5 over 3000 time steps. To achieve this consistency, 1×10^{-3} picoseconds was determined to be the maximum allowable time step for temperatures up to 1200° K, and this step size was used in most of the (N,V,E) ensemble runs.

24

The primary use of the (N,V,E) ensemble was to verify
that the Tersoff potential and positional derivatives
(forces) were correctly coded in the model. As a secondary
tool, the (N,V,E) simulation provided a cross-check of
results observed in the (N,P,H) ensemble described below.
The results of these cross-checks are discussed in Chapter
V.

(N,P,H) Ensemble. Since most laboratory
measurements are conducted in a constant pressure/constant
enthalpy environment, it is difficult to directly compare
the results of traditional (N,V,E) MD simulations with
effects observed in the laboratory. Fortunately, a
simulation method proposed by Anderson (2) and later
modified by Parrinello and Rahman (12) allows simulation of
an (N,P,H) ensemble. For a detailed explanation of the
development of this method, the reader is refered to the
cited articles. The Parrinello and Rahman, or P&R, method
was used extensively in this work, and a brief discussion
follows.

To allow the calculational cell to change shape, the
cell boundaries were defined by a set of mutable basis
vectors $\bar{a}$, $\bar{b}$, and $\bar{c}$, which made up the columns of a
transformation matrix $\overline{\overline{H}}$ (Figure 7). The atom positions were
then described by a set of reduced position vectors $\bar{s}_1$ so
that

$$\bar{r}_1 = \overline{\overline{H}} \, \bar{s}_1 \tag{12}$$
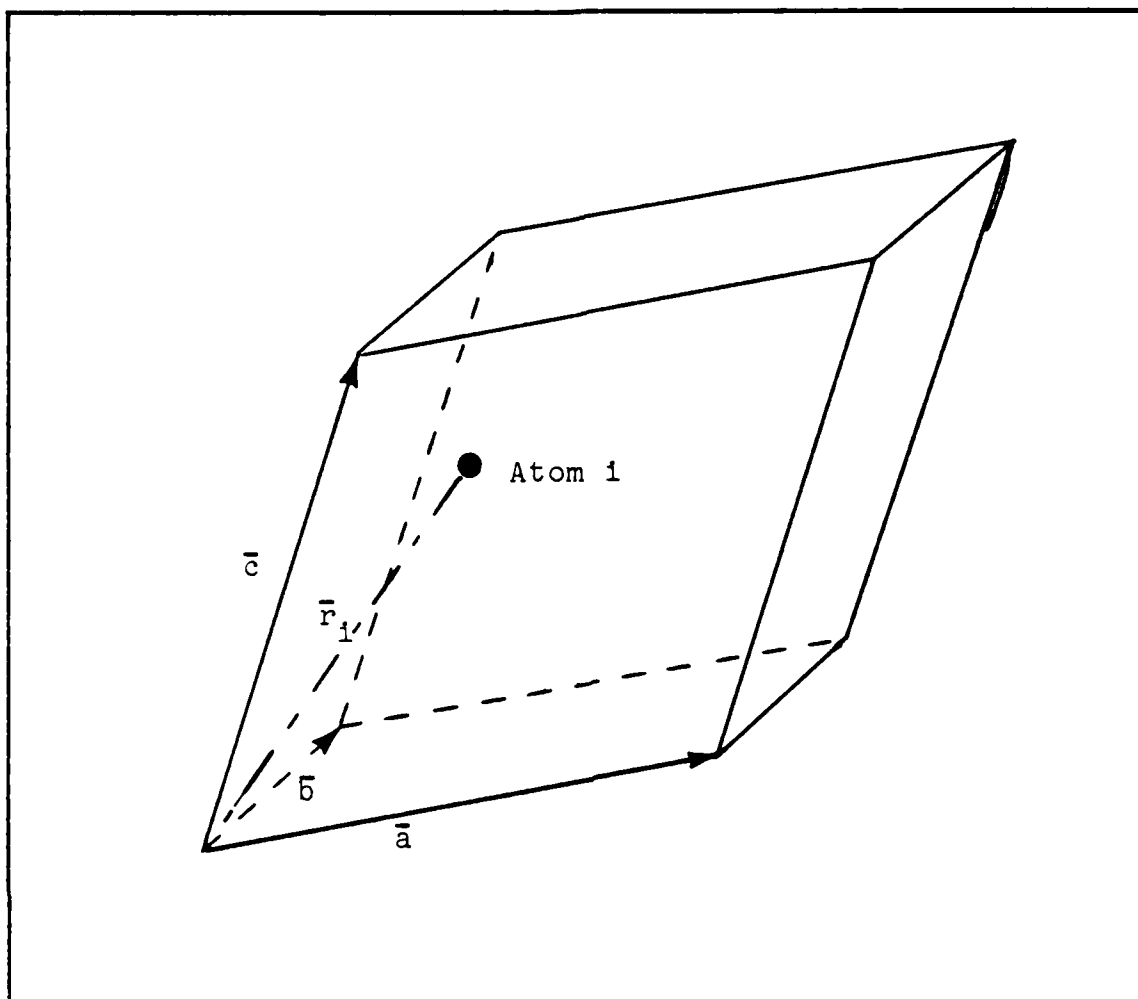
Figure 7: Basis Vectors of Computational Cell
for (N,P,H) Simulation (14:62)

The components of the reduced position vectors $\bar{s}_1$ range from
0 to 1. The volume Ω of the computational cell is simply
the determinant of the $\bar{\bar{H}}$ matrix.

$$\Omega = \|\bar{\bar{H}}\| \tag{13}$$

Changes in the structure of the computational cell are then
accomplished by altering the elements of the $\bar{\bar{H}}$ matrix in
response to the difference between the calculated internal
pressure and the constant external pressure. All runs for
this work were completed with no applied external pressure.

The Hamiltonian for this system as derived in the P&R article is merely the enthalpy of the system plus a term to include the kinetic energy of the walls of the computational cell. As pointed out in the reference article, the wall energy term is negligible, so that the enthalpy is a conserved quantity in this ensemble.

The P&R article describes the transformations necessary to solve Newton's equations in the reduced space, and to repeat the explanation here would provide no new insight. The interested reader is referred to the article listed in the Bibliography.

The desired consistency in the constant enthalpy simulation was set at 1 part in 10^4 over 3000 time steps. This was nearly achieved with a time step size of 2×10^{-4} picoseconds at 1200° K, and this time step size was used for the majority of the (N,P,H) ensemble runs.

Calculation of Properties

Many physical parameters, such as temperature, pressure, and internal energy, are dependent only on atomic positions and velocities. Therefore each possible atomic configuration (as defined by a unique set of N position vectors and N momentum vectors) has an associated set of these properties. Statistical mechanics calculates overall ensemble properties from expectation values based on the probability associated with each atomic configuration of the ensemble. However, the probability distribution function

27

for each of the infinite number of possible configurations
must be known to perform these calculations.

Fortunately, the ergodic hypothesis equates the
ensemble "average" properties (expectation values) to the
time average of the ensemble properties taken over many
time steps (ideally # of steps approaches ∞, but in practice
several thousand steps is sufficient). Therefore if a
sufficiently large data base exists, ensemble properties can
be calculated from a time-history of the atomic positions
and velocities, without knowing anything about the
associated configurations. The MD simulation provides the
needed time-history data to perform these calculations.

The instantaneous values of the temperature T, pressure
P, internal energy U and total energy E can be calculated
from the atomic positions and velocities as follows: (8,14)

$$T = \frac{m}{3Nk} \sum_i \bar{v}_i \cdot \bar{v}_i \qquad (14)$$

$$P = \frac{NkT}{V} - \frac{1}{3V} \sum_i \bar{r}_i \frac{dU}{d\bar{r}_i} \qquad (15)$$

$$U = \sum_i u(\bar{r}_i) \qquad (16)$$

$$E = \frac{m}{2} \sum_i \bar{v}_i \cdot \bar{v}_i + U \qquad (17)$$

In equations (14 - 17), k is Boltzmann's constant, V is volume, and m is the mass of the particles. All other variables are as previously defined.

Using the instantaneous properties calculated from the $\smile$ above equations, the ergotic hypothesis allows calculation of the ensemble "average" over L time steps by

$$\langle Property \rangle = \frac{1}{L} \sum_{n=1}^{L} Property(t_n) \qquad (18)$$

where $Property(t_n)$ is the instantaneous value of the property at the end of the n-th time step.

The summation term in equation (15) is called the virial. This is a term that appears often in the statistical mechanic calculations. Because of it's significance, Appendix B provides the derivation of the calculational form used in this computer simulation.

IV. Results of MD Runs

The MD runs completed in the course of this research can be separated into test runs, which were used to validate the coding of the potential and its positional derivatives, and primary runs, conducted to evaluate the performance of the potential. The results of both types of runs are presented in this chapter.

Results of Test Runs

The first set of tests performed were static evaluations (a single time step) conducted at 0° K to reproduce the bond energies for the rest bond lengths reported by Tersoff (17) for the dimer, diamond, simple cubic, and FCC structures. This was accomplished by setting the lattice constant in the model code so that the nearest neighbor distance matched the bond length associated with the structure under study. The number of atoms in the calculational cell was then adjusted to prevent undesired interactions with the "images" created by the periodic boundary conditions. The system energy was calculated by the MD program, and the value was divided by the number of atoms in the system to arrive at the energy per atom. Test run results are compared to Tersoff's values in Table III. The variance noted in the energy for the diamond structure is believed to be a result of a slight disagreement (about .0018 angstroms) in the rest bond length for that structure.

Table III. Calculated Bond Energy and Rest Bond Lengths for
            Dimer, Diamond, Simple Cubic, and FCC Structures

| Structure | Rest Bond Length (Angstroms) | Bond Energy (eV/atom) | |
		Current Work	Tersoff
Dimer	2.3132	-1.3117	-1.3117
Diamond	2.3518*	-4.6305	-4.6298
Simple Cube	2.5007	-4.2871	-4.2871
FCC	2.7298	-4.0818	-4.0818

* it is believed Tersoff's used a slightly smaller value

The bond lengths in Table III were found by calculating the
value of B_{ij} for each structure, then differentiating the
pair potential to determine the bond length of minimum
energy. Moreover, all other values match exactly,
confirming the correct installation of Tersoff's potential
in the model code.

Static calculations could not be used to validate the
force calculations in the model, so a single (N,V,E) run at
300° K with a time step of 1×10^{-3} picoseconds was
performed. A very small system (4 atoms) was used to
decrease the chance of fortuitous cancellation of errors,
and the simulation was performed for 5000 time steps. The
temperature, internal energy, and total energy are shown in
Figure 8. As predicted, the temperature and internal energy
are seen to oscillate about a mean value out of phase with

31
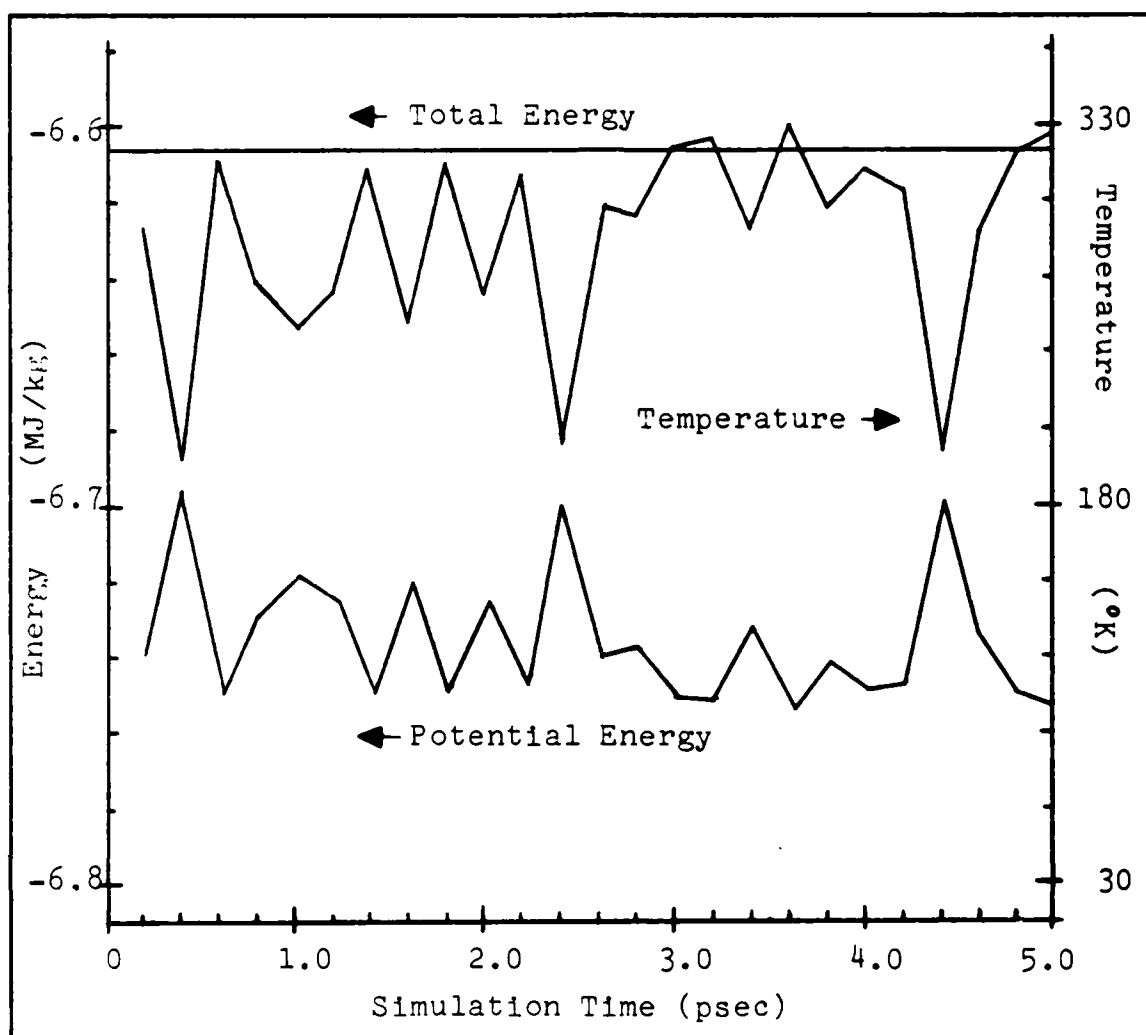
Figure 8: Temperature, Internal, and Total Energy vs. Time
(Instantaneous Values for 4 Atom N,V,E Ensemble
at 300 degrees K, dt = 1 femtosecond)

each other, and the total energy remains constant. This

provides very convincing proof of the correct evaluation of

the atomic forces, because only an exact balance of the

internal and kinetic energies will provide the consistency

observed.

Primary Simulation Runs

Four primary runs were conducted using the constant

enthalpy (N,P,H) ensemble to evaluate the applicability of

32

Table IV: Identification Number/Characteristics
of Primary MD Runs

ID #	Desired Temp (^{o}K)	Final Temp (^{o}K)	Scaling Steps	Resting Steps	Property Steps
1	300	303.3	200	500	2500
2	600	612.7	200	50	3000
3	900	853.2	50	150	2800
4	1200	1135.8	50	150	2800

the Tersoff potential in a molecular dynamic simulation.

All four runs were conducted at temperatures well below the

known melting temperature of silicon in a diamond structure

(1685° K), so that only solid silicon was modeled.

To facilitate the discussion of the results, each run

will be assigned an identification number. The identifying

number and characteristics of each run are recorded in Table

IV. All the runs were completed using a time step of 2 x

10^{-4} picoseconds. The differences in the number of scaling

and resting steps are a result of attempted optimization and

do not effect the final results.

In general, the results of the evaluation runs show the

Tersoff potential to be a well-behaved function. The state

variables of pressure, temperature, and internal energy show

random fluctuations about their respective mean values over

the period of simulation, as demonstrated by Figures 9 - 11.

The enthalpy values remain relatively constant, as expected,

and the instantaneous values are shown in Figure 12. Only

33
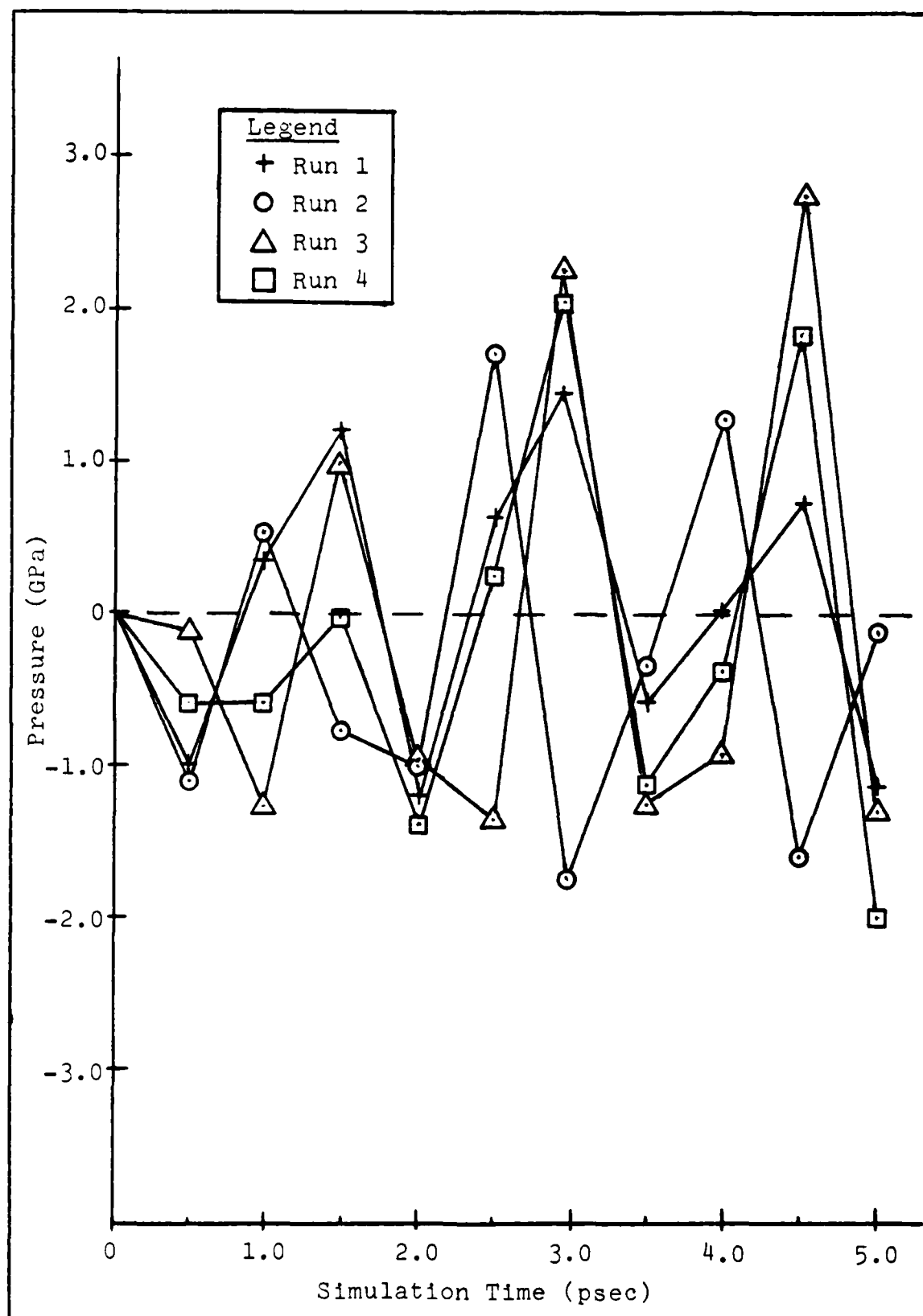
Figure 9:   Instantaneous Pressure vs. Time
for Primary Runs
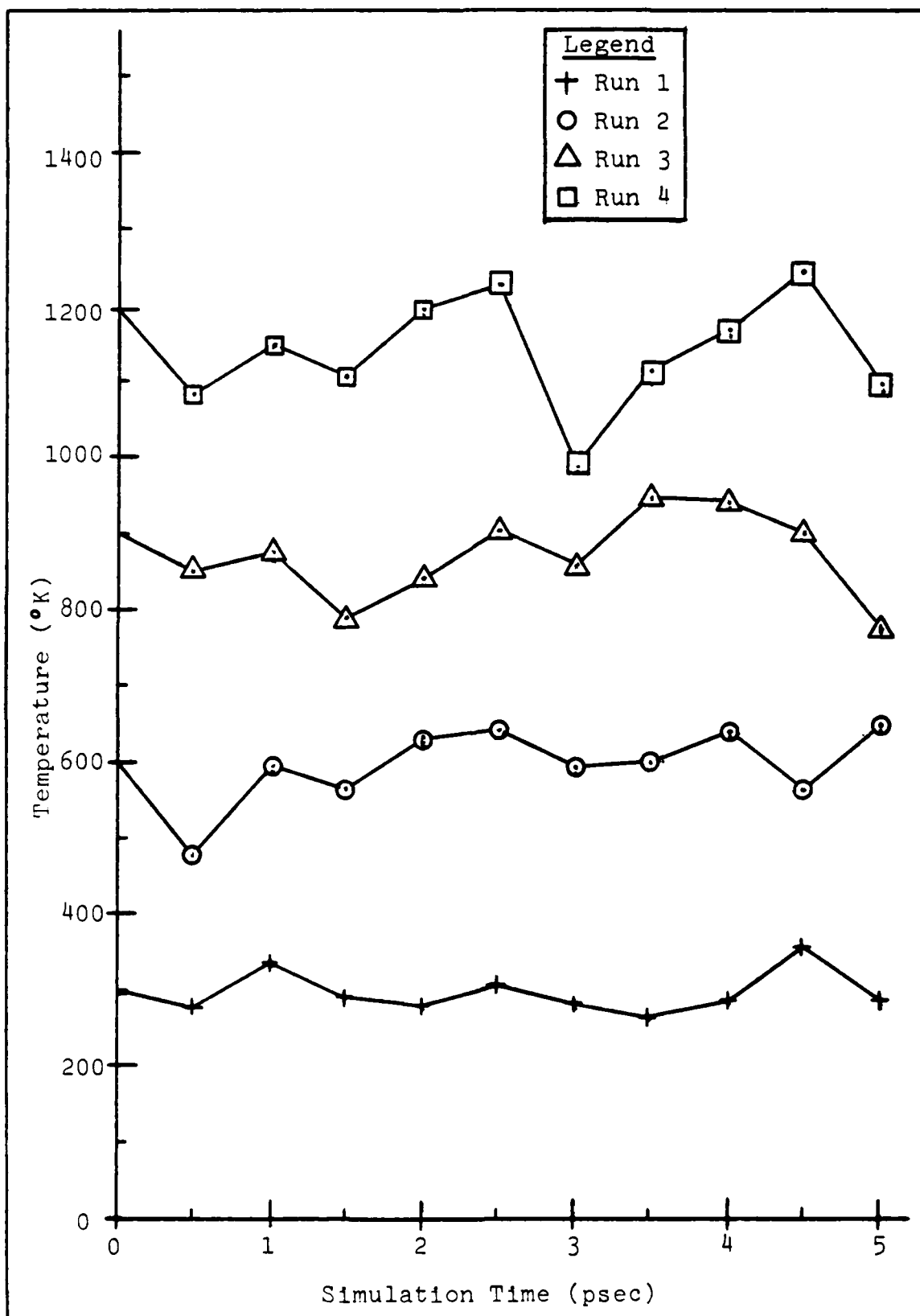
Figure 10:   Instantaneous Temperature vs. Time
             for Primary Runs
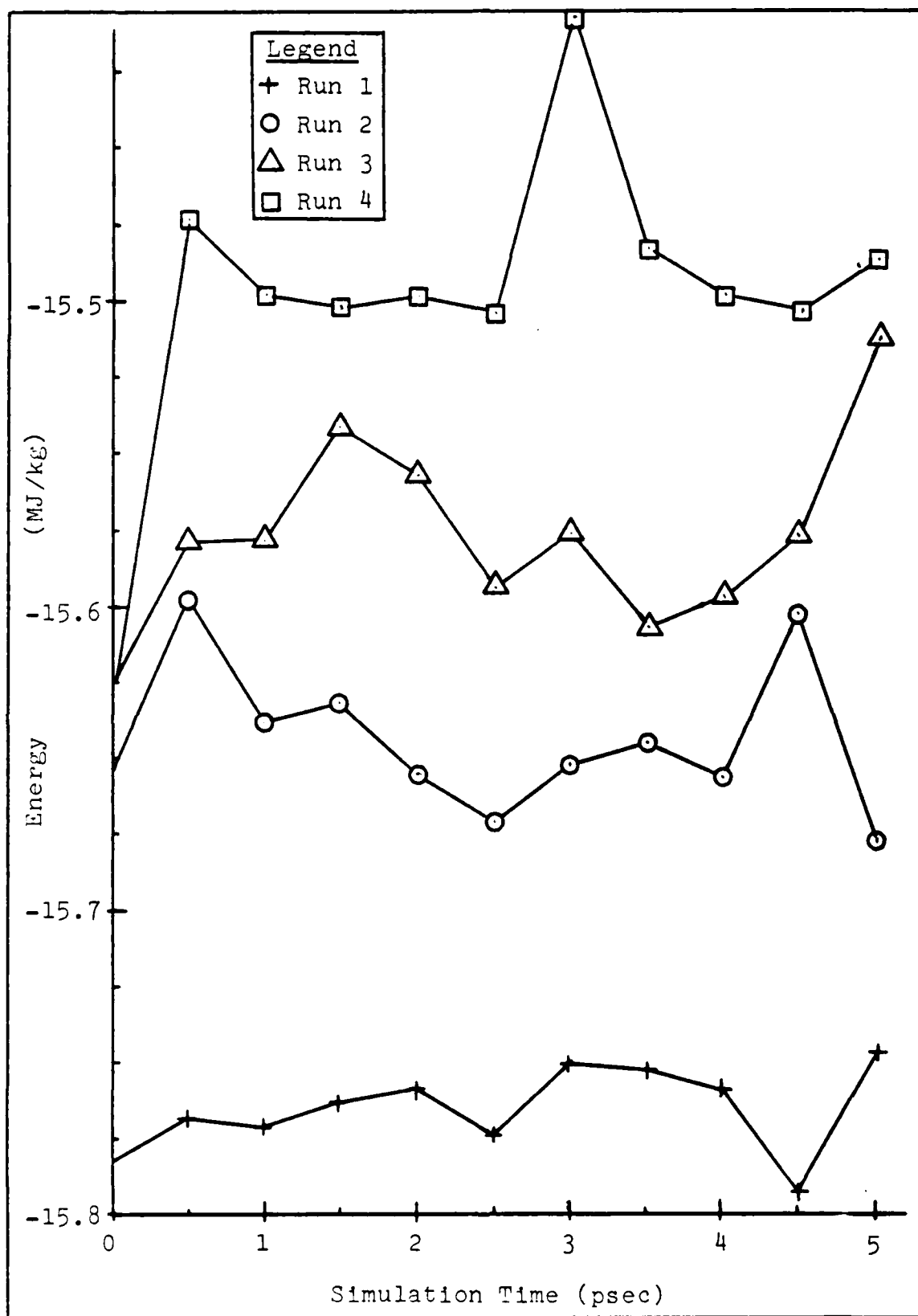
Figure 11:   Instantaneous Internal Energy vs. Time
for Primary Runs
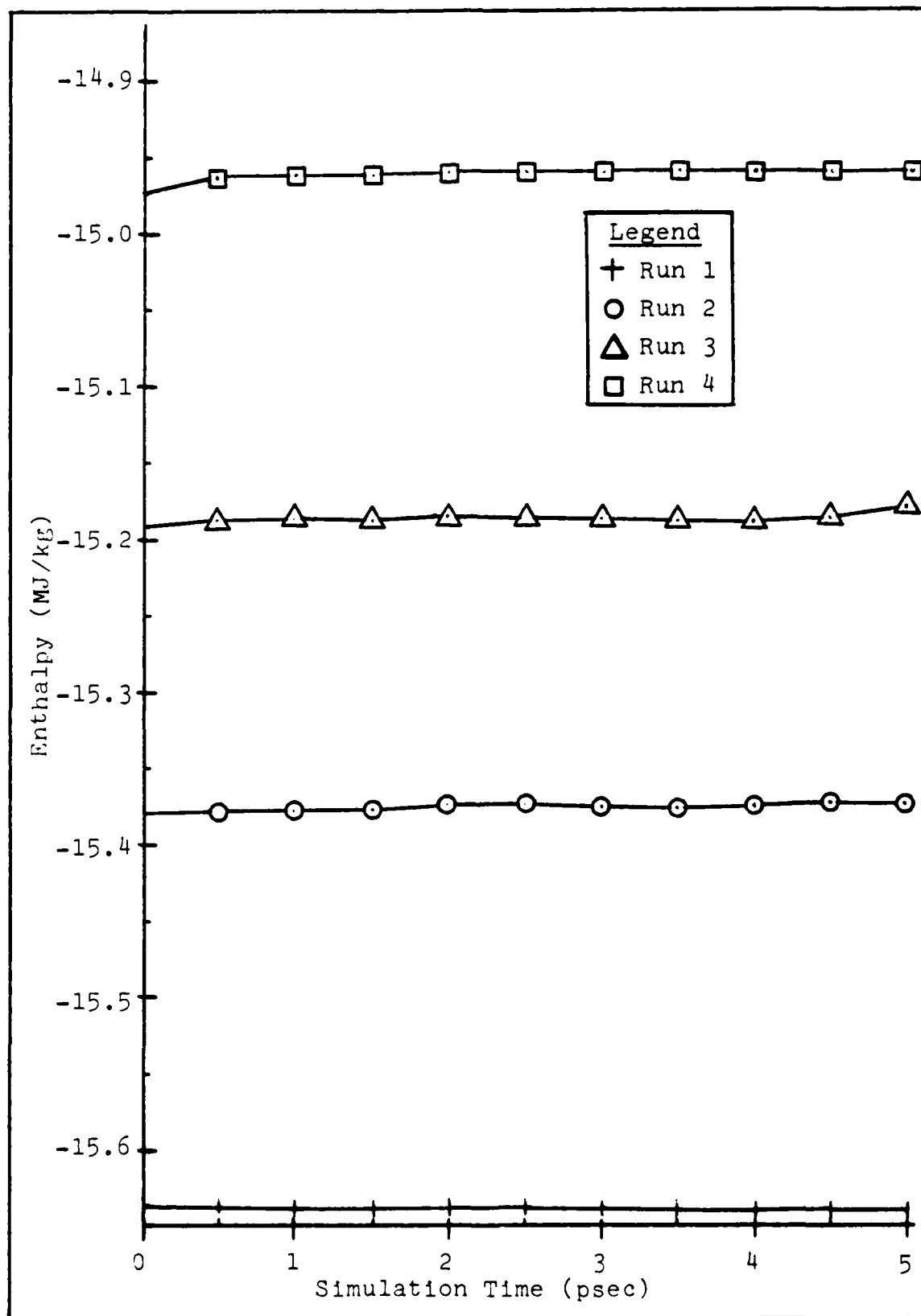
Figure 12: Instantaneous Enthalpy vs. Time
for Primary Runs
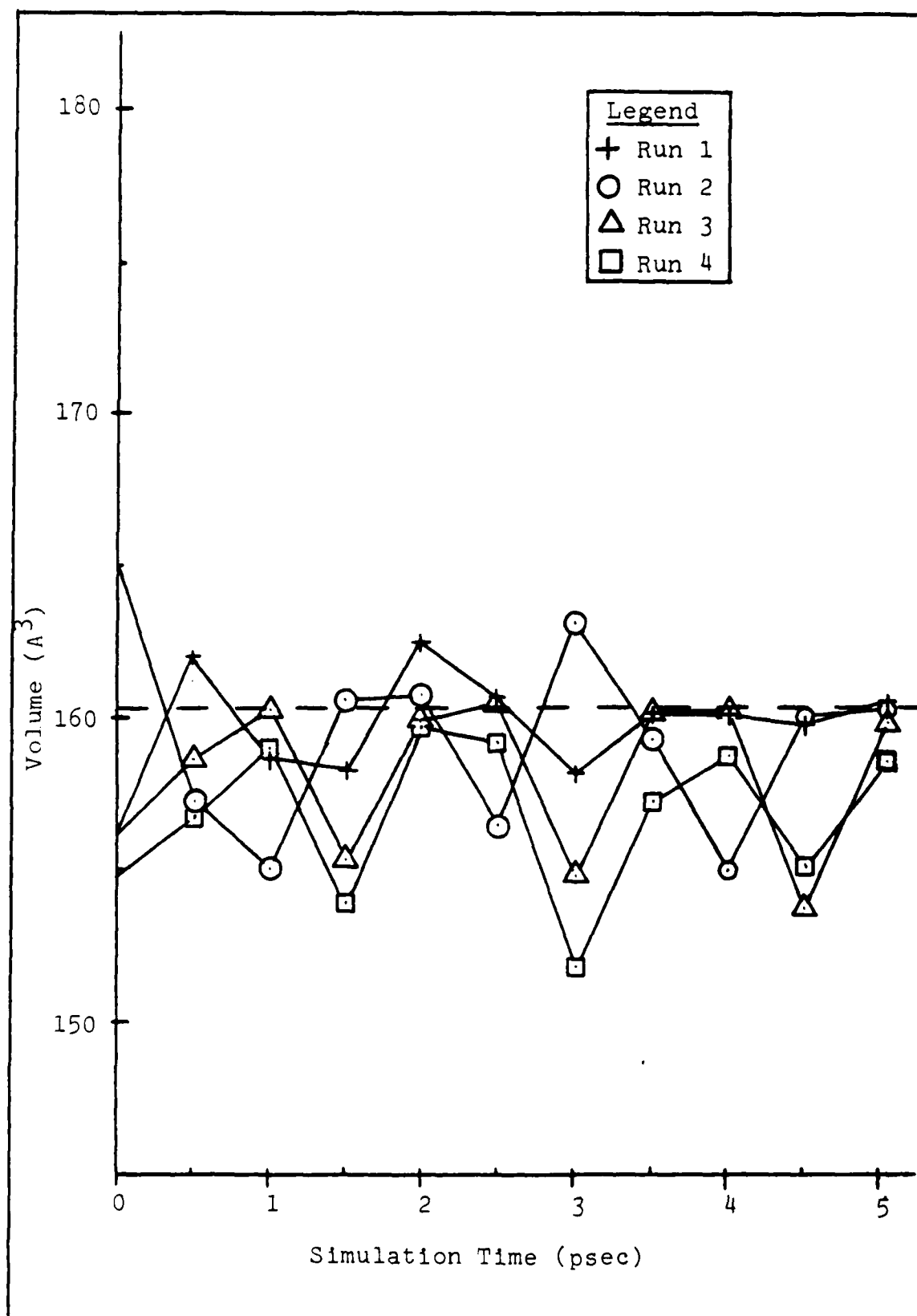
Figure 13:   Instantaneous Volume vs. Time
             for Primary Runs
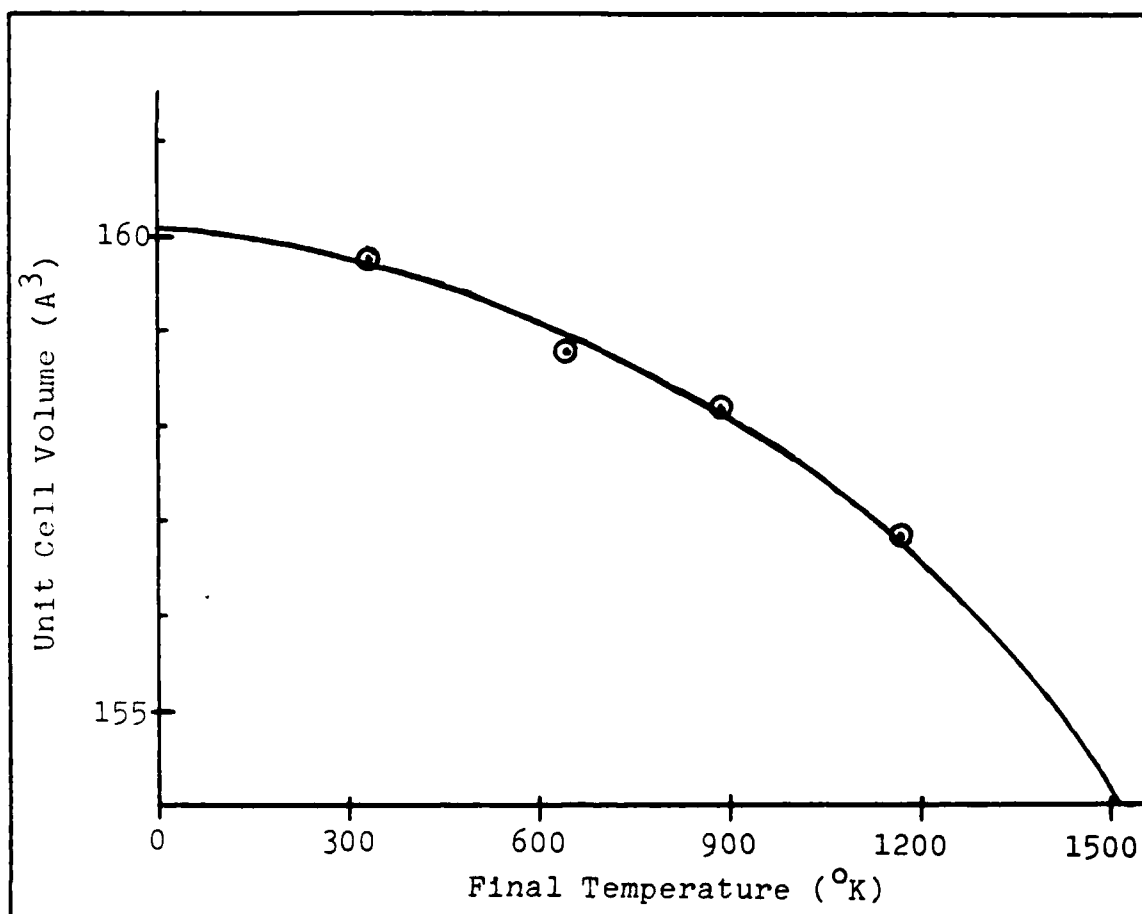
Figure 14:   Final Average Volume vs. Final Temperature
             of Primary Runs

the volume behaves in an unacceptable manner. From

experimental work, it is known that crystalline silicon

undergoes expansion when heated, until melting occurs (19).

A quick glance at Figure 13 makes it clear that this model

produces unrealistic behavior as the temperature is

increased, showing a marked decrease in the system volume as

the model is heated. To emphasize the temperature

dependence of this behaviour, Figure 14 shows the average

volume (after .56 psec simulation time) vs. the final

temperature with a spline fit connecting the data points.

The volume is seen to drop with increasing temperature, and

the slope of the volume vs. temperature curve becomes
increasingly negative. Investigation of this behavior is
the topic of Chapter V.

V. Investigation of Heat-Induced Shrinkage

The system shrinkage noted in the previous chapter is
even more severe than that reported by Thee on investigation
of Tersoff's earlier silicon potential (18). Thee reported
a similar decrease in system volume up to about 1000° K, at
which point the trend reversed itself and the system began
to expand. In this work, the volume loss showed no such
reversal over the temperature range examined (300 - 1200
degrees). The purpose of this chapter is to report the
results of tests run to verify the shrinkage problem and to
attempt to determine the cause of the shrinkage.

Confirmation of Problem

This research effort utilized a molecular dynamic
simulation code based on Thee's MD program. Therefore the
initial efforts to ascertain the cause of the shrinkage were
focused on confirming the problem; that is, insuring that
the calculational cell was indeed trying to shrink and that
the observed behavior was not due to a problem in the
computer code. If the shrinkage were caused by an error in
the (N,P,H) simulation portion of the code, repeating the
principal runs using (N,V,E) simulation should show a
positive pressure, indicating the system's desire to expand.
On the other hand, if the (N,V,E) simulation showed a
negative pressure, the inclination toward smaller volume
would be confirmed.

41

To test this hypothesis, a series of constant volume (N,V,E) runs were completed at 0, 300, and 1200° K using a range of lattice constants. The runs consisted of 1000 scaling steps for the 300° runs and 3000 scaling steps for the 1200° runs (2×10^{-4} psec time step). The initial atom positions and velocities for the 300° runs were the final values from the 300° principal run (Run #1), but the 1200° runs and the 0° runs were begun from normal lattice positions with appropriately scaled random velocities. Temperature scaling was applied each time step to insure the final temperatures would be as close as possible to the desired value so that the total energies could be compared.

The results of these runs are shown in Figures 15 and 16. The comparison of the final average pressures of the runs confirm the shrinkage displayed by the (N,P,H) principal runs. The final average total energies of many of the runs were too similar to allow conclusions to be drawn, even with the statistical base from 3000 time steps. It was determined that statistically significant energy differences would require unacceptably long runs, so no further attempts were made to determine the resultant energy differences.

Investigation into Cause of Shrinkage

In the Tersoff potential, the z_{ij} term is a complicated combination of environmental details that effect the bond strength. Differences in bond lengths, bonding angles, and total number of bonds all appear in the calculation of z_{ij}.
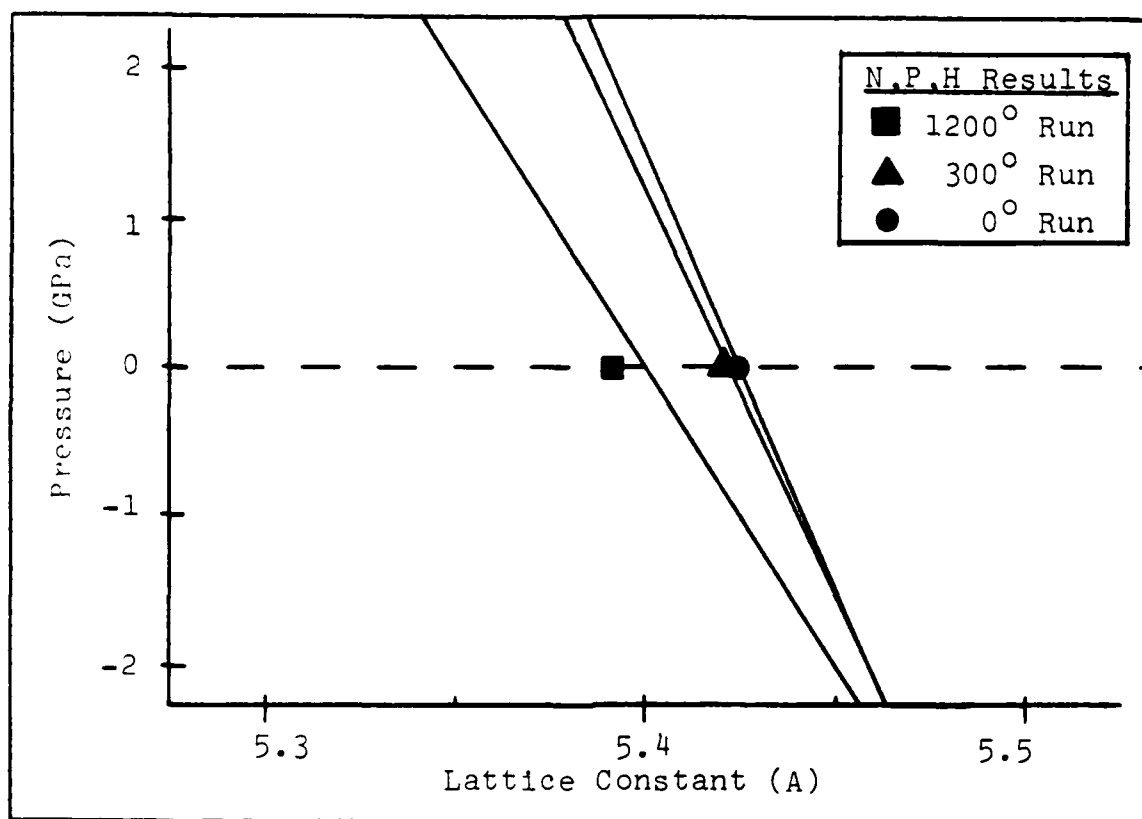
42

Figure 15: Final Average Pressure vs. Lattice Constant
for 0, 300, and 1200 Degree (N,V,E) Runs
(solid symbols annotate N,P,H result)
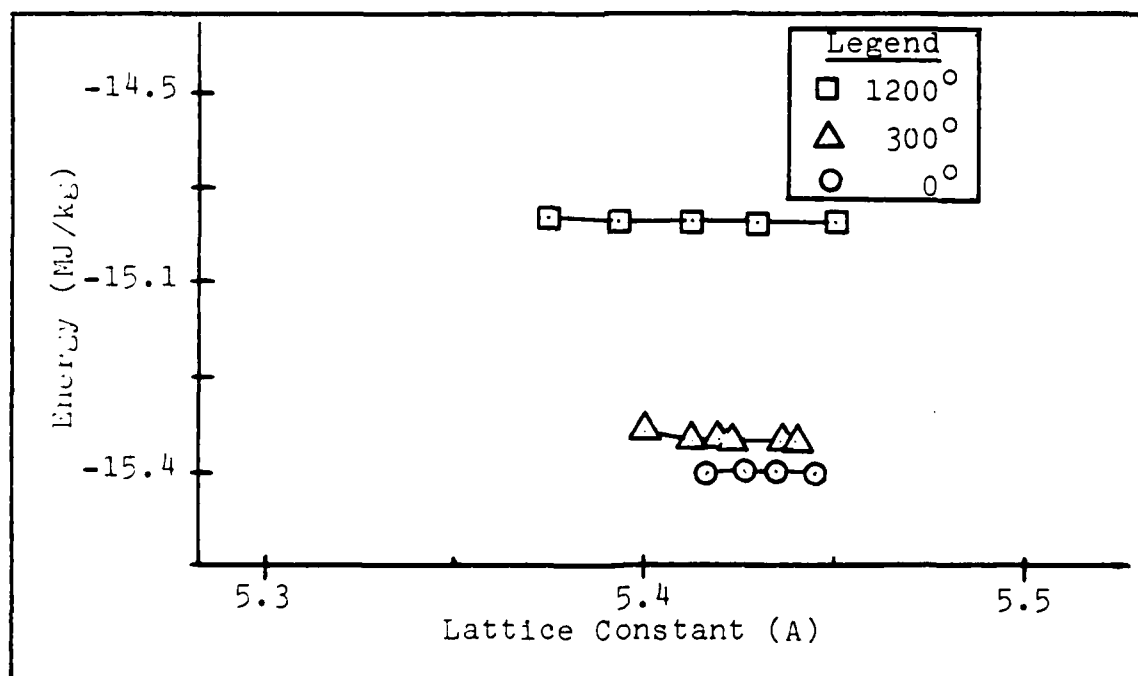
Figure 16: Final Average Total Energy vs. Lattice Constart
for 0, 300, and 1200 Degree (N,V,E) Runs

In an effort to determine the cause of the shrinkage phenomenon, these factors were examined individually in a series of tests that will be discussed in this section.

Difference in Bond Lengths. The difference in the length of the i-j bond compared to the i-k bond appears cubed in an exponent. As a result, one would expect this term to play a major role in determining the value of z_{ij}. To test the importance of this term, a (N,V,E) simulation at 600 degrees was performed with $\lambda_3 = 0$, which effectively removes the difference in bond lengths from the z_{ij} calculation. The run consisted of 500 scaling steps, 100 resting steps, and 4000 property steps with 2×10^{-4} psec time step. The results were compared with an identical run made with $\lambda_3 = 3.2394$. The final average pressure of both runs were identical (-0.59 GPa), and the final average total energies showed only a 0.2% difference. The small changes noted indicate that the differences in bond lengths must remain fairly small in the course of the simulation, so that removal of the term in an exponent has negligible effect. The bond length difference does not appear to be the driving force for the observed unrealistic behavior.

Angular Dependence of Bond Strength. The effect of the angle defined by the competing bonds was examined by calculating the value of z_{ij} for a single j-i-k triplet and the corresponding i-j bond energy for bonding angles between 0 - 180 degrees. The result is a surprisingly flat curve over a wide range of bonding angles (Figure 17). Caution
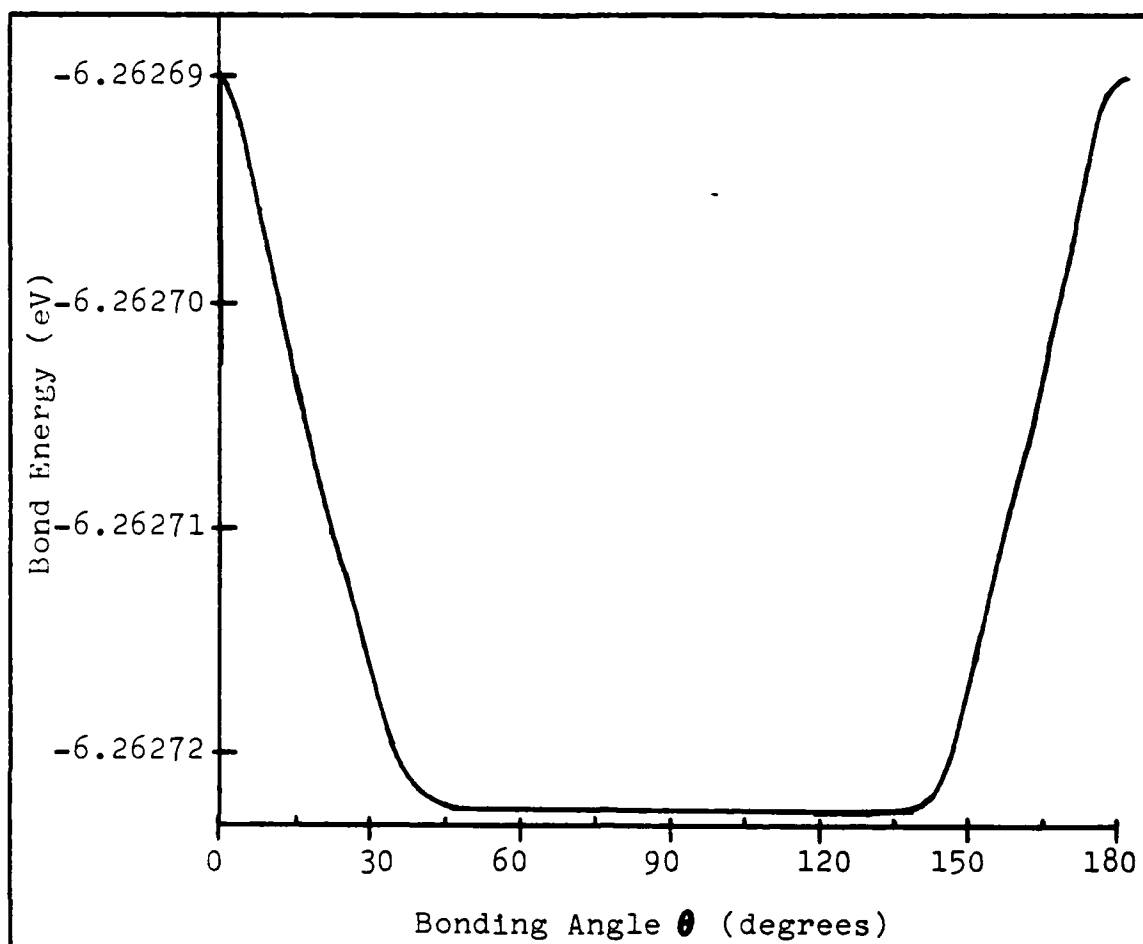
Figure 17:   Dependence of Single Bond Energy
              on Bonding Angle

must be applied when estimating the importance of this

result, however. Figure 17 shows only the change in a

single bond energy as a result of a single bond angle. In a

tetrahedrally bonded material (silicon in a diamond

lattice), change in any single bond angle effects the other

bond angles, and therefore the bond energies. The result of

this test does reinforce earlier statements concerning

Tersoff's dependence on coordination number rather than bond

angle to stabilize the diamond structure. In addition, the

results also hint that the relative insensitivity to bond
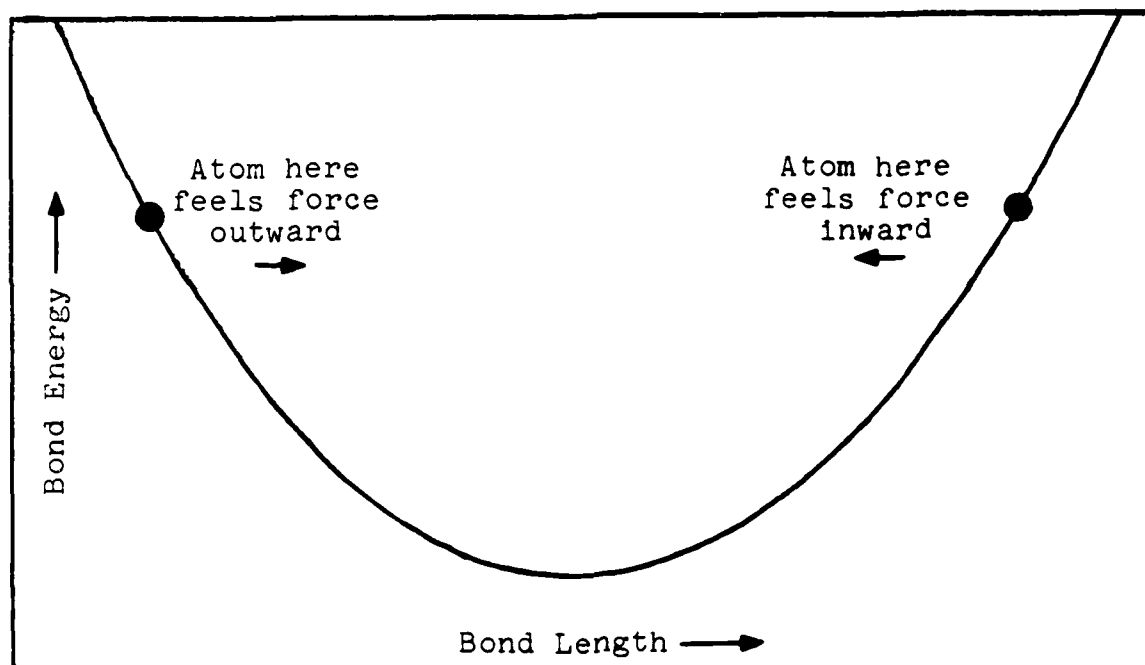
Figure 18:   Hypothetical Two-Dimensional Pair Potential
             (arrows show direction of restoring force)

angle may be part of the problem.   This possibility will be
discussed further in the final subsection on the unexplored
possibilities.

Effect of Constraining One Bondlength.   One final
series of tests was completed to examine the effect on the
total energy and volume of the calculational cell when one
single bond length within the cell is constrained to a given
value.   Before discussing the results of this test, a brief
explanation of the method of contraining one bondlength
is in order.

To understand the atom constraint, consider a two-
dimensional parabolic pair potential centered on some rest
separation distance between two atoms.   If an atom is
displaced from this rest position, it experiences a force
attempting to return it to the rest distance (Figure 18).
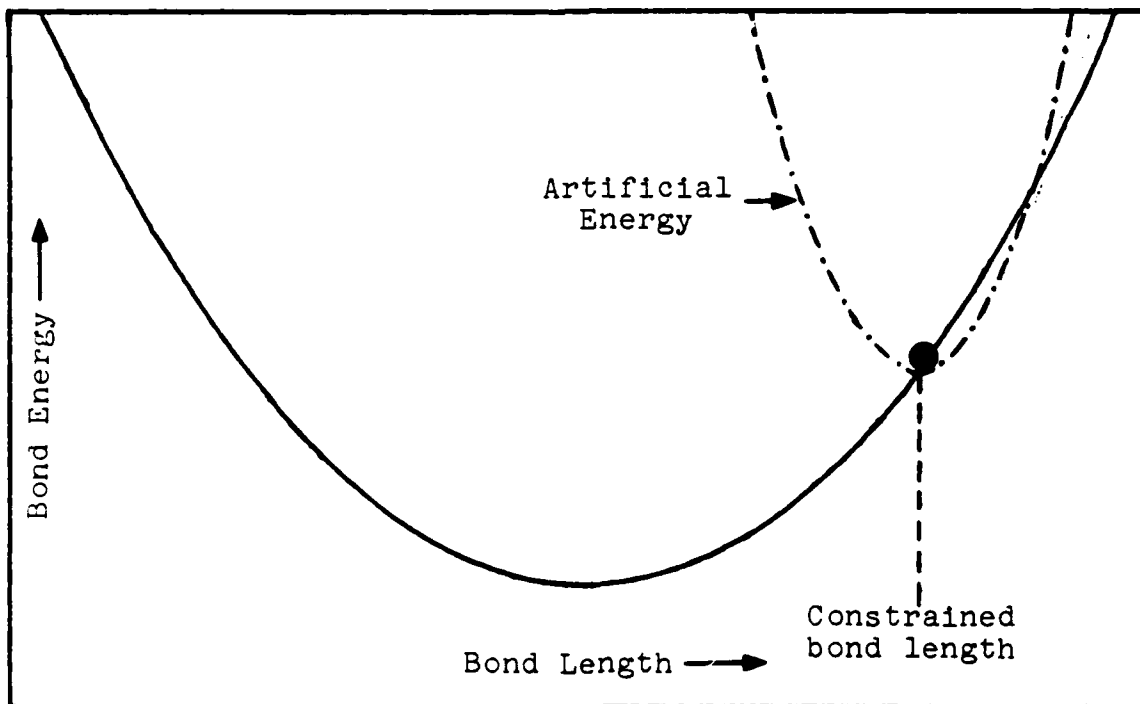
Figure 19: Hypothetical Two-Dimensional Pair Potential with
Superimposed Artificial Energy (no restoring force)

If an artificial parabolic energy curve centered on the
desired position is added to the pair potential, the atom no
longer experiences a restoring force and the bond distance
will be maintained (Figure 19). This is in essence the
technique used in these tests. The bond length between two
of the atoms is thus constrained, and the other atoms in the
computational cell are allowed to "relax" to find the lowest
energy state. The artificial energy is then removed and the
energy is calculated. The mechanics for this atomic
restraint method are outlined in Sabochick's dissertation,
and interested readers are referred there for more
information on the technique (14).

This series of tests was performed for a range of
restrained bond lengths and a variety of lattice constants.

Table V: Minimum Energy (eV) of a 64 Atom System with a
Single Constrained Bond

	Lattice Constant (Angstroms)				
Constrained Bond Length (Angstroms)	5.41	5.42	5.4312	5.44	5.45
2.117	-296.007	-296.037	-296.041	-296.024	-295.981
2.234	-296.202	-296.237	-296.248	-296.236	-296.199
2.352	-296.250	-296.291	-296.307	-296.298	-296.266
2.469	-296.200	-296.242	-296.261	-296.254	-296.224
2.587	-296.112	-296.159	-296.183	-296.180	-296.155

As one atom in the calculational cell is moved closer to a
neighboring atom, the moved atom should draw its other
neighbors with it, causing a slight decrease in the volume.
Conversely, as two atoms are held slightly apart, a slight
increase in the overall volume is expected. The data in
Table V shows the model behaving properly, with a slight
decrease in the lattice constant corresponding to the lowest
energy for constrained bond lengths less than the normal
2.352 Angstroms and a slight increase in the minimum energy
lattice constant for constrained bond lengths greater than
2.352 Angstroms. This tendency is more apparent in Figure
20, where a spline fit to the data for the constrained bond
lengths 2.117, 2.352, and 2.587 Angstroms shows the minimum
energy lattice constants to be approximately 5.427, 5.431,
and 5.435 Angstroms, respectively. Therefore the shrinkage
does not appear to be a result of an erroneous response by
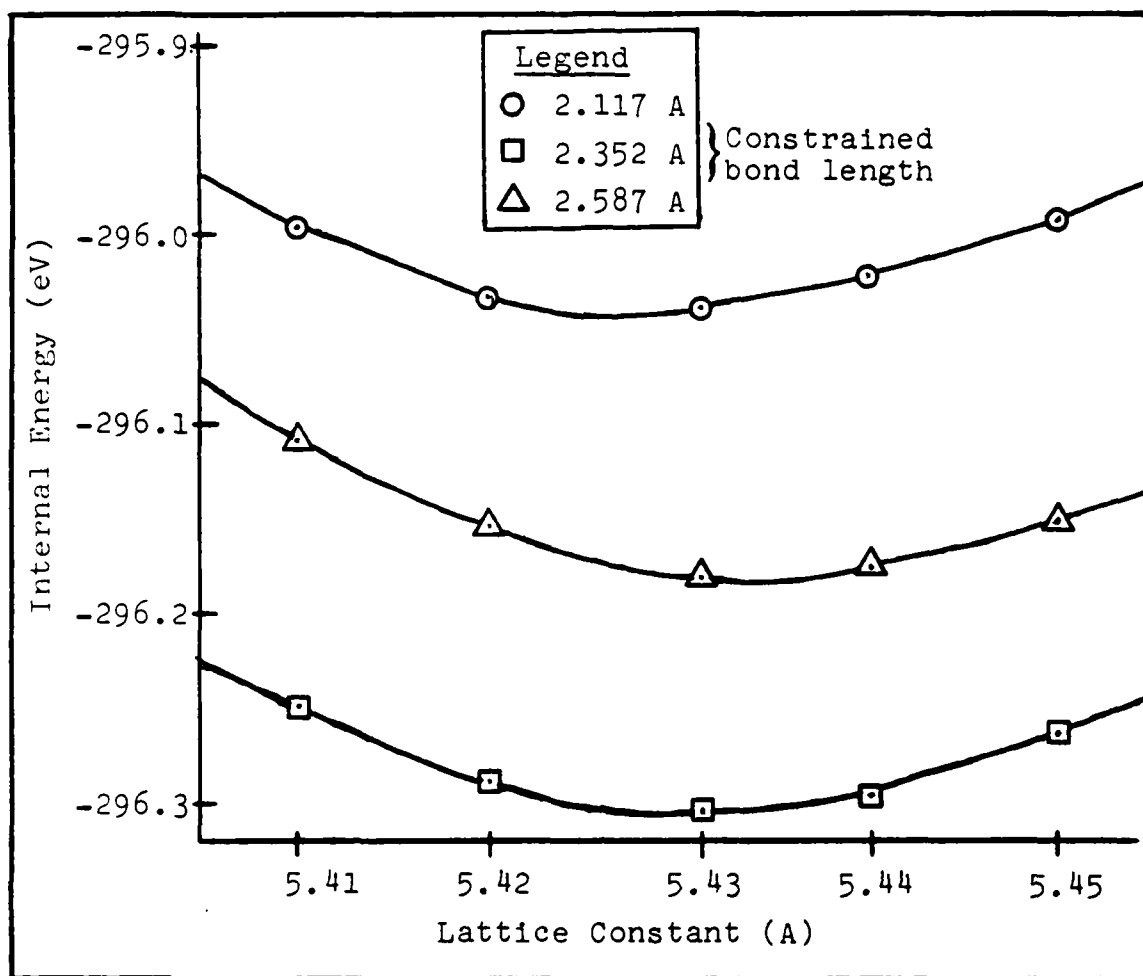
Figure 20:   Internal Energy vs. Lattice Constant with
              Constraint of a Single Bond Length
              (64 atom system)

the secondary neighbors to a change in separation distance

between two bonded atoms.

Unexplored Possibilities. While the evaluation tests

discussed in this chapter failed to positively identify the

cause of the observed shrinkage, they are by no means

exhaustive. The most promising clue to the weakness in the

potential lies in the relative unresponsiveness of the bond

energy to the bond angle, as discussed previously. A review

of the role of the z_{ij} term will help explain one possible

cause of the shrinkage.

Table VI: Coordination Number, z_{ij}, and Minimum Energy
Separation Distance for Diamond, Simple Cubic,
BCC, and FCC Structures

Structure	Coordination Number	z_{ij}	r_{min} (Ang)
Diamond	4	3.4373	2.3518
Simple Cube	6	6.0865	2.5007
BCC	8	8.9611	2.6018
FCC	12	14.628	2.7298

As pointed out in Chapter II, the bond strength is
modified by the bonding environment through a changing B_{ij}
value. This changing B_{ij} value is driven by a z_{ij} value
that is determined by the surrounding environment. For
periodic structures where all bond lengths are equal, it is
fairly simple to calculate the resulting z_{ij} value. Table
VI shows the coordination number and z_{ij} value associated
with the diamond, simple cubic, BCC, and FCC structures.
By taking the derivative of the Tersoff potential with
respect to the bond length r_{ij} while holding z_{ij} constant,
the minimum energy bond length for each value of z_{ij} can be
calculated from

$$r_{min} = \frac{\ln \frac{\lambda_1 A}{\lambda_2 B_{ij}}}{\lambda_1 - \lambda_2} \qquad (19)$$

These minimum bond lengths are recorded in Table VI. From equation (19) and the known relationship between z_{ij} and B_{ij} developed in Chapter II, it is apparent that a smaller value of z_{ij} equates to a larger B_{ij} and a therefore smaller minimum energy bond distance. Said more simply, the smaller z_{ij} becomes, the more compact the system becomes. This offers a possible explanation for the observed shrinkage, as explained below.

Consider a system containing four atoms. In the absence of directionally favored bonding, the atoms would be expected to occupy a planar arrangement with bond angles of 120 degrees and all bonds of equal length. This structure gives a z_{ij} value of 2.3139 and a corresponding r_{min} of 3.5172 Angstroms. If the structure is changed so that all three bonds are mutually orthogonal, the value of z_{ij} drops to 2.0 and r_{ij} becomes 2.3132 Angstroms, thereby allowing the system to shrink.

In a similar manner, it may be that the tetrahedral structure with identical bond lengths is not the structure corresponding to the lowest value of z_{ij}. Because of the extreme sensitivity of the z_{ij} term to coordination number, it is unlikely that any structure containing more than four nearest neighbors is energetically favored, but a different combination of bond angles and bond distances for the four neighbors of an atom may give a lower z_{ij} value. The existance of such a structure could easily be responsible for the shrinkage noted.

VI. Conclusions and Recommendations

Conclusions

The directional covalent bonding nature of silicon is very difficult to model accurately. Three-body potentials such as those proposed by Stillinger and Weber and Biswas and Hamann have shown some successful applications, but the strong dependency on the diamond structure limits their usefulness. The approach used in the new silicon potential proposed by Tersoff, explicit modeling of the bond environment, seems to be a more widely applicable model. The purpose of this research effort was to evaluate this new potential in a molecular dynamic study of solid silicon.

The Tersoff potential accurately reproduced the correct bonding lengths and bond energies for the diamond, simple cubic, and FCC structures of silicon in a static simulation $(0^\circ$ K). However, as the system was heated in a flexible boundary simulation, the volume decreased. This behavior is not observed in real silicon. Subsequent constant volume simulations confirmed that decreased volume yielded lower energy of the model when the simulation temperature was increased.

Investigative runs were completed in an effort to isolate the cause of the problem. The effect of unequal bond lengths, varying bond angles, and changing the length

of a single bond in a 64 atom system were examined, but none provided definitive identification of the source of the problem. The results of the bond angle tests suggested the possibility that, while Tersoff's potential accurately reproduces a most stable configuration having four nearest neighbors, the tetrahedral diamond structure may not be the lowest energy configuration.

Because of the unrealistic behavior under heating, the current Tersoff silicon potential is unusable for dynamic simulation.

Recommendations.

The generality of the Tersoff potential vis-à-vis the S&W three-body potential makes continued investigation of the Tersoff style of potential worthwhile. Two possible avenues of continued study are readily identified. The first is to experiment with the values of the 10 variables in the Tersoff potential by fitting the potential to dynamic properties such as the thermal expansion coefficient. Additional parameters may need to be added to accomplish this fitting. Indeed, simply increasing the cut-off radius slightly, say to 3.6 Angstroms (still less than the second-nearest neighbor distance in the diamond structure), might help prevent the shrinkage. Such a move would strengthen the angular dependence by limiting the distance one neighbor could move before interacting with, and subsequently raising the coordination number of, another neighboring atom.

53

A second possible extension would be to use the potential as it currently exists to perform a series of melting/annealing runs. The atom positions could be saved after each run in an attempt to identify low-energy configurations that might be responsible for the observed shrinkage. Dr. Tersoff has expressed interest in pursuing this action.

Throughout the course of this research, dialogue was maintained with the author of this potential. Continuing this interactive relationship offers an ideal opportunity for follow-on researchers to play a significant role in the development of a tool long awaited in the field - a general purpose silicon potential.

Appendix A: Derivation of Forces

The force F_n on any atom n is simply the negative
derivative of the internal energy U with respect to the
position of atom n, or

$$F_n = - \frac{d}{dr_n} U \qquad (20)$$

Although the vector notation has been omitted, equation (20)
actually represents three scalar equations, one for each
directional component. Since the form of each component
equation is identical, only one component is shown in this
appendix. The reader is expected to remember that parallel
equations apply to the other components.

While equation (20) appears simple enough, applying it
to Tersoff's potential can become confusing because of the
annotation method used. Therefore, before the derivatives
are discussed, an explanation of the terminology used in the
potential might be beneficial.

The basic geometry of the bond triad used in the
calculation of the bonding energy is shown in Figure 21.
The central premise of the Tersoff potential is that the
strength of the bond between any atoms i and j is affected
by the proximity to i of another atom k. Therefore for each
i-j-k bonding triad, there are positional derivatives and
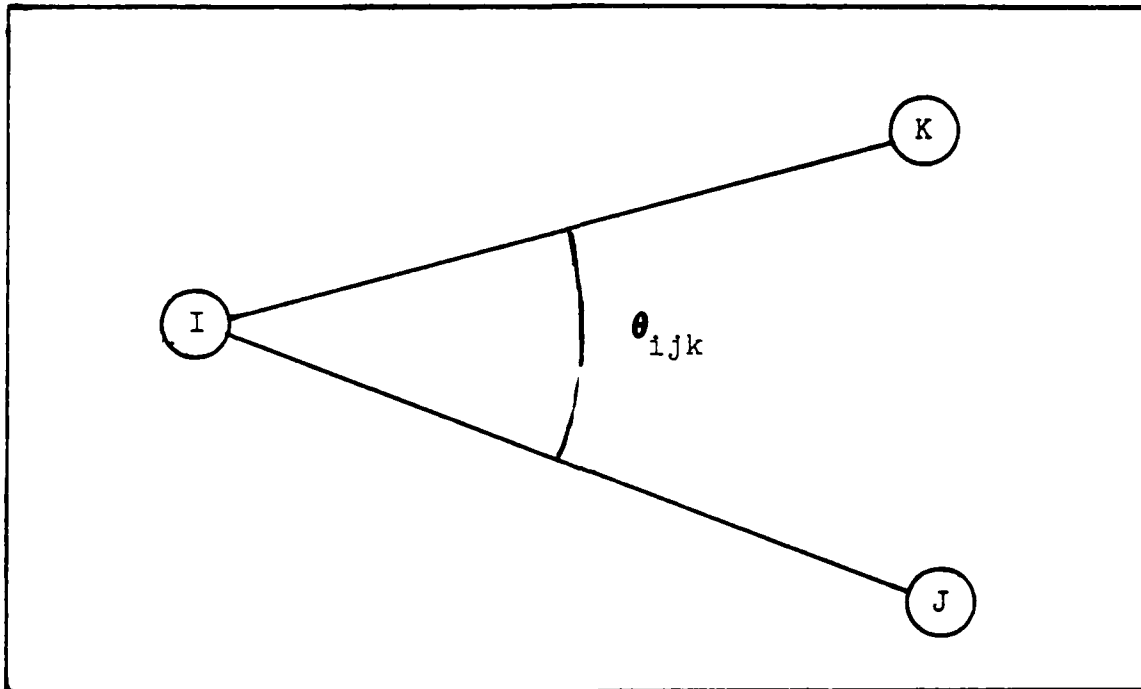
Figure 21: Geometry of Bonding Atoms in Tersoff's
Potential (18)

consequent forces acting on each of the three atoms.
Due to the lack of symmetry caused by the third body (k)
term, all three derivatives must be solved for separately.

The annotation used in the Tersoff potential may cause
some confusion in identifying the atoms. The "i-j-k"
designation of the potential must not be confused with the
"n" designation of equation (20). No single atom in the
system is just an i, j, or k atom; rather, all atoms are
all three, depending on which bond is being considered.
Figure 22 shows the dual annotation applied to the six
possible bonding triads for any three given atom positions.
For convenience, atoms 1, 2, and 3 were selected. Across
the top row of triads, atom 1 is atom i, atom j, and then
atom k, respectively. Therefore when the force on atom 1 is
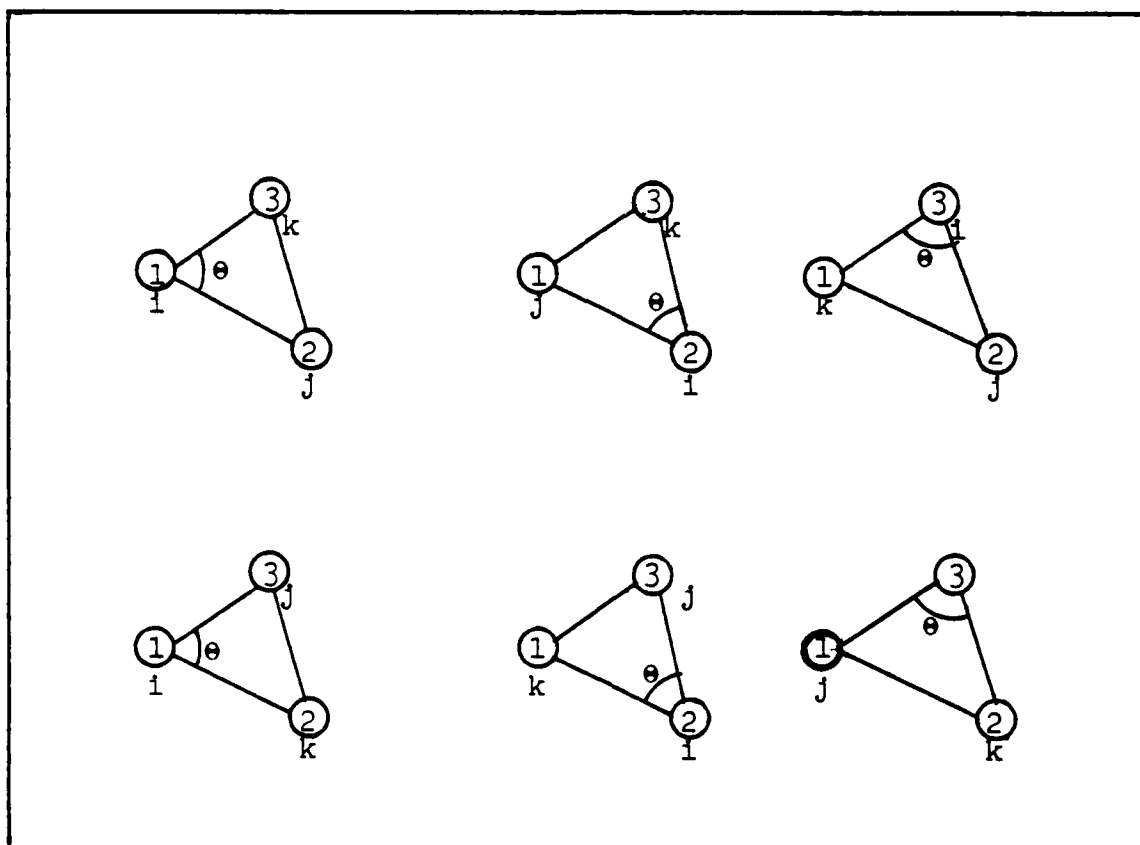
Figure 22: Six Bonding Triads Formed by Three-Atom System

calculated, it must be the sum of contributions from all the triads involved, so that

$$- F_n = \sum_{n,j,k} \frac{d}{dr_i} U + \sum_{i,n,k} \frac{d}{dr_j} U + \sum_{i,j,n} \frac{d}{dr_k} U \qquad (21)$$

where the first summation is over all triads where n is atom i, the second sum when n is atom j, and the third when n is atom k.

In the actual code, each triad is considered once, the dr_i, dr_j, and dr_k derivatives are evaluated, and the resulting forces are added to the previous forces for the

appropriate atom. Before each new time step begins, the
forces are reinitialized to zero.

The form of the Tersoff potential is

$$u(r_{1j}) = f_c(r_{1j})[A\exp(-\lambda_1 r_{1j}) - B_{1j}\exp(-\lambda_2 r_{1j})] \qquad (3)$$

$$f_c(r) = \begin{cases} 1 & r < R - D \\ .5 - .5\sin[\dfrac{\pi(r - R)}{2D}] & R - D < r < R + D \\ 0 & r > R + D \end{cases} \qquad (4)$$

$$B_{1j} = B_0(1 + bz_{1j}^n)^{-1/(2n)} \qquad (5)$$

$$z_{1j} = \sum_{k \neq i,j} f_c(r_{1k})\, g(\theta)\, \exp(-[\lambda_3(r_{1k} - r_{1j})]^3) \qquad (6)$$

$$g(\theta) = 1 + c^2/d^2 - c^2/[d^2 + (\cos\theta + h)^2] \qquad (7)$$

Successive application of the chain rule can be used to find

$$\frac{d}{dr_1} U = \frac{d}{dr_{1j}} U \frac{dr_{1j}}{dr_1} + \frac{d}{dr_{1k}} U \frac{dr_{1k}}{dr_1}$$

$$\frac{d}{dr_j} U = \frac{d}{dr_{1j}} U \frac{dr_{1j}}{dr_j} + \frac{d}{dr_{jk}} U \frac{dr_{jk}}{dr_j}$$

$$\frac{d}{dr_k} U = \frac{d}{dr_{1k}} U \frac{dr_{1k}}{dr_k} + \frac{d}{dr_{jk}} U \frac{dr_{jk}}{dr_k}$$

58

These three equations can be simplified somewhat by

reverting to component annotation and recalling that

$$r_{ij} = [\ (r_i^x - r_j^x)^2 + (r_i^y - r_j^y)^2 + (r_i^z - r_j^z)^2 \ ]^{1/2}$$

In terms of the x component, it is apparent that

$$\frac{dr_{ij}}{dr_i^x} = - \frac{dr_{ij}}{dr_j^x} = \frac{r_i^x}{r_{ij}}$$

and that similar equations apply to the other derivatives,

giving

$$\frac{dr_{ik}}{dr_i^x} = - \frac{dr_{ik}}{dr_k^x} = \frac{r_i^x}{r_{ik}}$$

and

$$\frac{dr_{jk}}{dr_j^x} = - \frac{dr_{jk}}{dr_k^x} = \frac{r_j^x}{r_{jk}}$$

Therefore only the three potential derivatives remain to be

determined.

Before proceeding with the derivatives of U directly,

it might be more convenient to get rid of the theta term.

59

Using the Law of Cosines, the angle can be related to the distances separating the atoms to give

$$\cos\theta = \frac{r_{1j}^2 - r_{1k}^2 + r_{1k}^2}{2r_{1j}\,r_{1k}}$$

Taking the required derivatives gives

$$\frac{d\cos\theta}{dr_{1j}} = .5[1/r_{1k} - r_{1k}/r_{1j}^2 + r_{jk}^2/(r_{1j}^2\,r_{1k})]$$

$$\frac{d\cos\theta}{dr_{1k}} = .5[1/r_{1j} - r_{1j}/r_{1k}^2 + r_{jk}^2/(r_{1j}\,r_{1k}^2)]$$

$$\frac{d\cos\theta}{dr_{jk}} = -r_{jk}/(r_{1j}\,r_{1k})$$

Continuing along these lines, the chain rule can be used to determine the desired derivatives of the g function, giving

$$\frac{dg(\theta)}{dr_{1j}} = \frac{dg(\theta)}{d\cos\theta}\frac{d\cos\theta}{dr_{1j}}$$

with similiar functions for the r_{1k} and r_{jk} derivatives. The second term of these parallel equations is already known, and the first term is simply

$$\frac{dg(\theta)}{d\cos\theta} = 2c^2(\cos\theta + h)/[d^2 + (\cos\theta + h)^2]^2$$

The product of these terms removes the theta variable from the calculations, leaving the derivatives of the g function with respect to r_{1j}, r_{1k}, and r_{jk}.

Returning now to the derivatives of the potential, the differentiation of a product can be applied to give

$$\frac{d}{dr_{1j}} U = \frac{d}{dr_{1j}} f_c(r_{1j})[A\exp(-\lambda_1 r_{1j}) - B_{1j}\exp(-\lambda_2 r_{1j})]$$

$$+ f_c(r_{1j})[-\lambda_1 A\exp(-\lambda_1 r_{1j}) + \lambda_2 B_{1j}\exp(-\lambda_2 r_{1j})$$

$$- \frac{d}{dr_{1j}} B_{1j}\exp(-\lambda_2 r_{1j})]$$

$$\frac{d}{dr_{1k}} U = - f_c(r_{1j})\frac{d}{dr_{1k}} B_{1j}\exp(-\lambda_2 r_{1j})$$

$$\frac{d}{dr_{jk}} U = - f_c(r_{1j})\frac{d}{dr_{jk}} B_{1j}\exp(-\lambda_2 r_{1j})$$

Looking first at the derivative of the cut-off function,

$$\frac{d}{dr} f_c(r) = - \frac{\pi}{4D} \cos[\frac{\pi}{2}(r - R)/D]$$

Determining the derivative with respect to r_{1j} is simply a matter of inserting the value of r_{1j} into the equation for r and solving.

The derivatives of B_{1j} are somewhat more involved, since B_{1j} is a function of all three variables. Once again the chain rule is applied, yielding

$$\frac{d}{dr_{1j}} B_{1j} = \frac{d}{dz_{1j}} B_{1j} \frac{d}{dr_{1j}} z_{1j}$$

$$\frac{d}{dr_{1k}} B_{1j} = \frac{d}{dz_{1j}} B_{1j} \frac{d}{dr_{1k}} z_{1j}$$

$$\frac{d}{dr_{jk}} B_{1j} = \frac{d}{dz_{1j}} B_{1j} \frac{d}{dr_{jk}} z_{1j}$$

Again the first term in all three equations is equivalent. Solving for this derivative of B_{1j} gives

$$\frac{d}{dz_{1j}} B_{1j} = B_0 (-(1 + bz_{1j}^n)^{-1+1/(2n)} /2) bz_{1j}^{(n-1)}$$

Only the derivatives of z_{1j} remain to be solved for. One final time the chain rule is applied to give

$$\frac{d}{dr_{ij}} z_{ij} = \sum_{k \neq i,j} \left\{ f_c(r_{ij}) \exp(-[\lambda_3(r_{ik} - r_{ij})]^3) \frac{d}{dr_{ij}}g(\theta) \right.$$

$$+ f_c(r_{ik}) \, g(\theta) \exp(-[\lambda_3(r_{ik} - r_{ij})]^3)$$

$$\left. * \, 3\lambda_3 [\lambda_3(r_{ik} - r_{ij})]^2 \right\}$$

where all terms on the right side of the equation are included in the summation over k. Likewise for the r_{ik} and r_{ij} derivatives,

$$\frac{d}{dr_{ik}} z_{ij} = \sum_{k \neq i,j} \left\{ f_c(r_{ik}) \exp(-[\lambda_3(r_{ik} - r_{ij})]^3) \frac{d}{dr_{ik}}g(\theta) \right.$$

$$+ f_c(r_{ik}) \, g(\theta) \exp(-[\lambda_3(r_{ik} - r_{ij})]^3)$$

$$* \, -3\lambda_3 [\lambda_3(r_{ik} - r_{ij})]^2$$

$$\left. + \frac{d}{dr_{ik}} f_c(r_{ik}) \, g(\theta) \exp(-[\lambda_3(r_{ik} - r_{ij})]^3) \right\}$$

and

$$\frac{dz_{ij}}{dr_{jk}} = \sum_{k \neq i,j} \left\{ f_c(r_{ik}) \exp(-[\lambda_3(r_{ik} - r_{ij})]^3) \frac{d}{dr_{jk}}g(\theta) \right\}$$

At this point all the values are known, and back substitution can be used to obtain the forces on each atom

of a triad. When these forces are summed over all the
triads an atom is involved in, the result is the total force
experienced by that atom.

Appendix B: Calculation of Virial Term

Kittel defines the virial term used in the pressure
calculation as (10:223,224)

$$VT = \sum_i \bar{F}_i \cdot \bar{r}_i$$

For the Tersoff potential, this can be expressed as

$$VT = \sum_{\substack{i,j \neq i \\ k \neq i,j}} r_i F^i_{ijk} + r_j F^j_{ijk} + r_k F^k_{ijk}$$

where F^i_{ijk} is the force on atom i due to the ijk bond triad,
F^j_{ijk} is the force on atom j, and F^k_{ijk} is the force on atom
k.   The summation is then over all bonding triads.   Note
that vector notation has been repressed for convenience.

This may look like a more complex form, but it can be
converted to a form that is independent of translation.
This is accomplished by application of Newton's third law,
according to which the total forces in the bonding triad
must equal zero, or

$$F^i_{ijk} + F^j_{ijk} + F^k_{ijk} = 0$$

Multiplying the above equation by r_i, subtracting the
product from the virial term, and repeating these steps for
every ijk bonding triad gives

$$VT = \sum_{\substack{i,j \neq i \\ k \neq i,j}} (r_j - r_i) F^j_{ijk} + (r_k - r_i) F^k_{ijk}$$

This is the calculational form used in the MD program. Notice that the position vectors have been replaced by a difference, which removes the translation dependence.

Bibliography

1. Alder, B. J. and T. W. Wainwright, *Journal of Chemistry and Physics,* 31, 459 (1953).

2. Andersen, Hans C. "Molecular Dynamics Simulation at Constant Pressure and/or Temperature," *J. Chem. Phys.,* 72 (4): 2384-2393 (15 February 1980).

3. Biswas R. and D. R. Hamann. "Interatomic Potentials for Silicon Structural Energies," *Physical Review Letters,* 55 (19): 2001-2004 (4 November 1985).

4. Blaisten-Barojas, Estela and D. Levesque. "Molecular-Dynamics Simulation of Silicon Clusters," *Physical Review B,* 34 (6): 3910-3916 (15 September 1986).

5. Dodson, Brian W. "Evaluation of the Stillinger-Weber Classical Interaction Potential for Tetragonal Semiconductors in Nonideal Atomic Configurations," *Physical Review B,* 33 (10): 7361-7363 (15 May 1986).

6. Egami, T., K. Maeda, and V. Vitek. "Structural Defects in Amorphous Solids: A Computer Simulation Study," *Philosophical Magazine A,* 41 (6): 883-901 (1980).

7. Gibson, J. B. and Others, "Dynamics of Radiation Damage," *Physical Review,* 120 (4): 1229-1253 (15 November 1960).

8. Haile, J. M. *A Primer on the Computer Simulation of Atomic Fluids by Molecular Dynamics.* Clemson University, 1980. (unpublished).

9. Johnson, R. A. "Calculations of Small Vacancy and Interstitial Clusters for an FCC Lattice," *Physical Review,* 152 (2): 629-634 (9 December 1966).

10. Kittel, C. *Elementary Statistical Physics.* New York: John Wiley & Sons, Inc., 1958.

11. Lam, N. Q., N. V. Doan, and L. Dagens. "Multiple Defects in Copper and Silver," *J. Phys. F: Met. Phys,* 15: 799-808 (1985).

12. Parrinello, M. and A. Rahman. "Polymorphic Transition in Single Crystals: A New Molecular Dynamics Method," J. Appl. Phys., 52 (12): 7182-7190 (December 1981)

13. Pearson, E. and Others. J. Cryst. Growth, 70:33 (1985)

14. Sabochick, Michael. Atomistic simulation Study of Vacancy Clusters in Copper. PhD dissertation. Massachusetts Institute of Technology, Cambridge, MA, 1985.

15. Stillinger, Frank H. and Thomas A. Weber. "Computer Simulation of Local Order in Condensed Phases of Silicon," Physical Review B, 31 (8): 5262-5271 (15 April 1985).

16. Tersoff, J. "New Empirical Model for the Structural Properties of Silicon," Physical Review Letters, 56 (6): 632-635 (10 February 1986).

17. Tersoff, J. Personal Correspondence. IBM Research Center, Yorktown Heights, NY. (October 1986).

18. Thee, Paul. Calculation of the Equation of State for Silicon. MS Thesis. School of Engineering, Air Force Institute of Technology (AU), Wright-Patterson AFB OH, December 1986.

19. Touloukian, Y. S. and Others. Thermophysical Properties of Matter, Volume 13: Thermal Expansion, Nonmetallic Solids. New York: IFI/Plenum, 1977.

20. Vitek, V., S. P. Chen, and T. Egami. "Molecular Dynamics Study of Atomic-Level Structural Parameters in Liquid and Amorphous Metals," Journal of Non-Crystalline Solids, 61 & 62: 583-588 (1984).

Captain William D. Metzler was born on 23 April 1954 in
Colby, Kansas. He graduated from high school in Brewster,
Kansas, in 1972 and accepted an appointment to the United
States Air Force Academy in Colorado Springs, Colorado.
Upon graduation, he was awarded a Bachelor of Science in
Chemistry and a regular commission in the United States Air
Force. He completed Undergraduate Navigator Training and
received his wings in March of 1977. He then attended
Electronic Warfare Training, and performed as instructor and
evaluator Electronic Warfare Officer in both the B-52H and
RC-135S aircraft. He entered the School of Engineering, Air
Force Institute of Technology, in September, 1985.

                    Permanent address: P. O. Box 26

                                          Brewster, Kansas   67732

REPORT DOCUMENTATION PAGE

1a REPORT SECURITY CLASSIFICATION	1b RESTRICTIVE MARKINGS
UNCLASSIFIED	

2a. SECURITY CLASSIFICATION AUTHORITY	3. DISTRIBUTION/AVAILABILITY OF REPORT
	APPROVED FOR PUBLIC RELEASE;
2b DECLASSIFICATION/DOWNGRADING SCHEDULE	DISTRIBUTION UNLIMITED

4 PERFORMING ORGANIZATION REPORT NUMBER(S)	5 MONITORING ORGANIZATION REPORT NUMBER(S)
AFIT/GNE/ENP/87M-5	

6a. NAME OF PERFORMING ORGANIZATION	6b OFFICE SYMBOL (If applicable)	7a. NAME OF MONITORING ORGANIZATION
School of Engineering	AFIT/ENP	

6c. ADDRESS (City, State, and ZIP Code)	7b. ADDRESS (City, State, and ZIP Code)
Air Force Institute of Technology Wright-Patterson AFB, Ohio 45433	

8a. NAME OF FUNDING/SPONSORING ORGANIZATION	8b. OFFICE SYMBOL (If applicable)	9 PROCUREMENT INSTRUMENT IDENTIFICATION NUMBER

8c. ADDRESS (City, State, and ZIP Code)	10. SOURCE OF FUNDING NUMBERS			
	PROGRAM ELEMENT NO	PROJECT NO	TASK NO	WORK UNIT ACCESSION NO

11. TITLE (Include Security Classification)
EVALUATION OF TERSOFF'S REVISED SILICON POTENTIAL IN A MOLECULAR DYNAMIC SIMULATION OF SOLID SILICON

12 PERSONAL AUTHOR(S)
William R. Metzler, B.S., Capt, USAF

13a. TYPE OF REPORT	13b TIME COVERED	14 DATE OF REPORT (Year, Month, Day)	15. PAGE COUNT
MS Thesis	FROM _____ TO _____	1987 March	80

16 SUPPLEMENTARY NOTATION

17.	COSATI CODES		18. SUBJECT TERMS (Continue on reverse if necessary and identify by block number)
FIELD	GROUP	SUB-GROUP	Molecular Dynamics, Silicon

19 ABSTRACT (Continue on reverse if necessary and identify by block number)

Thesis Chairman: Michael J. Gabechick, Captain, USAF
Assistant Professor of Nuclear Engineering
Air Force Institute of Technology (AFIT/ENP)

Approved for public release; IAW AFR 190-1.
LYNN E. WOLAVER
Dean for Research and Professional Development
Air Force Institute of Technology (AFIT)
Wright-Patterson AFB OH 45433

20 DISTRIBUTION/AVAILABILITY OF ABSTRACT	21 ABSTRACT SECURITY CLASSIFICATION
☒ UNCLASSIFIED/UNLIMITED ☐ SAME AS RPT ☐ DTIC USERS	UNCLASSIFIED

22a NAME OF RESPONSIBLE INDIVIDUAL	22b TELEPHONE (Include Area Code)	22c OFFICE SYMBOL
Michael J. Gabechick, Captain, USAF	513-255-	AFIT/ENP

DD Form 1473, JUN 86 Previous editions are obsolete

A modified silicon potential proposed by Tersoff was evaluated in a molecular dynamic simulation of diamond silicon at temperatures well below the melting point. Four temperatures between 0 K and 1200 K were modeled using a constant enthalpy ensemble of 64 atoms.

At all temperatures above 0 K, the simulation displayed increasing atom density with increasing temperature. This behavior is physically unrealistic and makes the Tersoff potential unsuitable for molecular dynamic simulation.

A variety of tests were performed using both constant volume and constant enthalpy ensembles in an effort to determine the characteristic of the Tersoff potential responsible for thermally-induced shrinkage, but results were negative.

END

5-87

DTIC